Politecnico di Torino

Department of Environmental, Land and Infrastructure Engineering



Master of Science in Georesources and Geoenergy Engineering

A.Y. 2024/2025

Optimization of Oil Production Adopting Improved /Enhanced Oil Recovery Methods Via 3D Numerical Simulation Approach

Supervisor: Candidate:
Professor Vera Rocca Hatem Eisa (s329220)

November 20, 2025

This page has intentionally been left blank.

Acknowledgements

"The saying of Prophet Muhammad (peace be upon him), 'Seek knowledge from the cradle to the grave,' has been a constant source of motivation for me. This timeless wisdom has shaped my commitment to learning and has deeply influenced the effort I devoted to completing this thesis."

I would like to express my deepest gratitude to my family for their unwavering support and encouragement throughout this journey.

I am profoundly thankful to the high management of Eni North Africa, particularly the Managing Director and the Division Staff Manager, for their continuous trust, guidance, and the opportunity to pursue this work.

I would like to express my heartfelt gratitude to my supervisor, Professor Vera Rocca, for her encouragement, support, crucial guidance, and patience throughout my Master of Science journey. I am fortunate to have had such a helpful supervisor.

I want to thank my friends, especially Jawdat Abd Al Karim, for his substantial help and collaboration, and to all my other colleagues for their support and insights during these past two years.

Abstract

The optimisation recovery from mature resources requires the integration of various modelling resources and geological knowledge. This thesis addresses the challenge of maximising recovery from a mature, compartmentalised offshore reservoir, focusing on the Norne Field (Norwegian Sea). The study's objective is to quantify the incremental value of Improved/Enhanced Oil Recovery (IOR/EOR) options. The production from Norne field started in 1997, both water and gas injection began 1998 and field oil production reached the maximum around 34000 sm3/day. In 2002 the oil field production started to decline and 2005 the gas injection ceased. The total number of production wells is 23, and 11 injectors, with emphasis on optimised waterflooding using a reproducible 3D numerical-simulation workflow. The workflow integrates (i) black-oil dynamic simulation in ECLIPSE reservoir simulator (ECLIPSE 100, SLB) with history-consistent controls and field constraints (e.g., injector/producer limits, BHP caps, water-cut and GOR cut-offs), and (ii) scenario design and ranking based on pressure support and incremental recovery. Three forwardforecast scenarios (Nov-2006 to Jan-2020) are tested: a do-nothing base case; targeted new producers selected by remaining-oil and interference criteria; and producer additions combined with strategically placed injectors to improve areal sweep. Results show cumulative oil recovery rising from ~73.3×10⁶ Sm³ (base) to ~74.7×10⁶ Sm³ with added producers, and up to ~77.2×10⁶ Sm³ when new injectors are included—while sustaining higher average reservoir pressure and acceptable water-handling, subject to a field injection capacity of ~42,000 Sm³/d.

Comparing to the base case, there is an increase in an incremental recovery factor (ΔRF) of + 0.9 % with added producers and + 2.4 % with added injectors. The analysis indicates that infill production coupled with injector placement delivers the largest, most robust uplift for Norne-type reservoirs, providing practical guidance for life-extension planning in mature North Sea assets.

This study demonstrates that integrating static characterization with dynamic simulation is essential for designing an effective IOR strategy and improving hydrocarbon recovery. In our case, dynamic modelling indicates that the recovery factor increases from 45.8% in the base case (Scenario A) to 48.3% in the best-performing case (Scenario C), which reinforces the waterflood through a combination of new producers and injectors. These results provide actionable guidance for extending the productive life of mature fields.

Contents

Acknowledgements	3
Abstract	4
List of Figures	8
List of Tables	10
Scope of Work	11
1. Introduction	14
2. Theoretical Background	16
2.1 Primary reservoir drives and production mechanisms	16
2.2 IOR vs EOR methods	18
2.3 Basic concepts of waterflooding (IOR method)	20
2.3.1 Voidage Replacement Ratio (VRR)	23
2.3.2 Waterflooding Patterns	25
2.3.3 Fluid Properties	26
2.4 Buckley Leverett Frontal Advance Calculation	26
3. Model Characterization	28
3.1 Numerical Simulation and Modelling	28
3.2 Static Model	29
3.2.1 Reservoir Description	30
3.3 Dynamic Model	33

3.3.1 Dynamic model construction	33
3.3.2 Reservoir Production and Pressure History	34
4. Forecast Scenarios : results and Discussion	41
4.1 Scenario A: Do nothing	41
4.2 Scenario B: Do nothing + new production wells	49
4.3 Scenario C: Scenario B(option 7) + new injection wells	63
5. Conclusion and Future Work	72
6. References	74

List of Figures

Figure 1: Water injectivity variation (Craig, 1971)	22
Figure 2: Common waterflood-pattern configurations	25
Figure 3: Norne field Location	29
Figure 4: Fluid in place Regions	30
Figure 5: Stratigraphical sub-division of Norne Reservoir	32
Figure 6: field oil production rate (Model vs History)	34
Figure 7:Total field oil production rate (Model vs History)	35
Figure 8: Field water production rate (Model vs History)	36
Figure 9: Field water injection rate (Model vs History)	37
Figure 10: Field gas production rate (Model vs History)	38
Figure 11: Field gas injection rate (Model vs History)	39
Figure 12:Location of existing wells	42
Figure 13: Field Pressure vs Time (scenario A)	43
Figure 14: Field oil production rate (scenario A)	44
Figure 15: Field Cumulative Oil Production vs Time (scenario A)	45
Figure 16: Field Gas Production vs Time (scenario A)	46
Figure 17: Field Cumulative Gas Production vs Time (scenario A)	47
Figure 18: Field water production rate vs Time (scenario A)	48
Figure 19:Field Cumulative water Production vs Time (scenario A)	48
Figure 20: Field water injection rate vs Time (scenario A)	49
Figure 21:Field Pressure vs Time (scenario B)	52

Figure 22: Field oil production rate (scenario B)
Figure 23:Field Cumulative Oil Production vs Time (scenario B)
Figure 24:Field Gas Production vs Time (scenario B)
Figure 25:Field Cumulative Gas Production vs Time (scenario B)
Figure 26: Field water production rate vs Time (scenario B)
Figure 27:Field Cumulative water Production vs Time (scenario B)
Figure 28: Field water injection rate (scenario B)
Figure 29: Field Cumulative water injection vs Time (scenario B)
Figure 30: Layer 7 Oil Saturation (Nov 2006): P-19 target area and remaining-oil accumulation 58
Figure 31:Layer 7 Oil Saturation (Jan 2020): Depletion of the P-19 remaining-oil accumulation 59
Figure 32: Layer 9 Oil Saturation (Nov 2006): P-10 target area and remaining-oil accumulation 60
Figure 33:Layer 9 Oil Saturation (Jan 2020): Depletion of the P-10 remaining-oil accumulation 60
Figure 34:Layer 11 Oil Saturation (P-15 Target Area): Nov 2006 vs Jan 2020
Figure 35: Layer 11 Oil Saturation (Jan 2020): Depletion of the P-15 remaining-oil accumulation 61
Figure 36: Location of injection wells
Figure 37: Field Pressure vs Time (scenario C)
Figure 38: Field oil production rate (scenario C)
Figure 39: Field Cumulative Oil Production vs Time (scenario C)
Figure 40: Field Gas Production vs Time (scenario C)
Figure 41: Field Cumulative Gas Production vs Time (scenario C)
Figure 42: Field water injection rate (scenario C)
Figure 43:Field Cumulative water production vs Time (scenario C)
Figure 44: Field water injection rate vs Time (scenario C)

List of Tables

Table 1: Types of EOR Methods (Muggeridge et al., 2014)	. 19
Table 2: Types of IOR Methods(Muggeridge et al., 2014)	.20
Table 3:Norne Field Key Properties	.31
Table 4:Reservoir HOIP and Production	.40
Table 5: Cumulative oil production and cumulative additional oil scenario B	. 50
Table 6: Cumulative oil production, cumulative additional oil, and cumulative water production	.51
Table 7: Cumulative oil production and cumulative additional oil scenario C	. 63
Table 8: Cumulative oil production, cumulative additional oil, and cumulative water production	
scenario C	. 64
Table 9: Final results for all scenarios	.71

Scope of Work

This thesis assesses options for Improved Oil Recovery (IOR) at the depleted Norne Field, Norwegian Sea, to increase hydrocarbon recovery from mature reservoir parts. The field is located ~80 km north of Heidrun and at a water depth of ~380 m, it was discovered in 1992 and came on stream on 6 November 1997, through a FPSO connected to several subsea templates. The main oil zone is found in the Jurassic Ile and Tofte formations (gas also in Not/Garn) at ~2,500–2,700 m TVD, under a long-standing water-injection process.

Norne is chosen as reference case because: (i) a well-documented, open benchmark 3D black-oil model (NORNE_ATW2013) allows for reproducible research and scenario testing; (ii) the field is richly documented publicly (technical background: history-matching/optimization studies and 4D seismic) which can be used to robustly validate the simulation results; and (iii) it is representative of subsea, compartmentalized geology and late life waterfloods typical for many North Sea assets where the placement of injectors/producers and management of voidage become critical

The work encompasses the following components:

• **Dynamic reservoir simulations** are conducted with ECLIPSE 100 (black-oil) to evaluate IOR strategies under realistic operational constraints and surveillance limits.

Norne—~80–85 km north of Heidrun in ~380 m water depth, discovered in 1992 and on stream since 6 Nov 1997 via an FPSO with subsea templates—was chosen because

(i) a public, benchmark 3D black-oil deck (NORNE ATW2013) enables fully

reproducible experiments; (ii) the field has rich open literature on production/4D seismic history matching for validation; and (iii) its mature waterflood, compartmentalization, and subsea setting are representative of late-life North Sea assets where injector/producer placement and voidage management dominate performance.

• Comparative Scenario Analysis

Three development scenarios are designed and evaluated over a 13-year forecast window (Jan-2007 to Jan-2020), using the history-consistent state at the end of 2006 as the starting point. All scenarios honor facility limits (oil/water handling and field injection capacity), well operating constraints Bottom hole pressure /Bottom hole temperature, water cut /Gas oil ratio cut-offs, and regulatory envelope (max drawdown/pressure, injector fracture-risk margin).

- a. Do-Nothing (Basecase): Continuation of existing operations without new wells or pattern changes. Controls mirror late-2006 settings (producer BHP limits, current injector targets). Purpose: provide the reference trajectory for pressure decline, water cut trend, and base recovery against which uplift is measured.
- b. New production Wells: Selective drilling of additional producers to accelerate and access remaining oil in poorly drained compartments. The placement rules are the minimum distances to faults and existing wells; landing in high-NTG rock types and preference for segments with strong pressure support.

c. New injection wells: Drilling of additional injectors is proposed to maintain reservoir pressure and improve areal/vertical sweep across compartments. Candidate injector locations are screened using remaining-oil saturation maps and depletion/pressure diagnostics, then refined through a dedicated sensitivity study that tests alternative injector placements alongside the producers already defined in previous step. The selected configuration maximizes recovery and pressure support while respecting facility constraints for water treatment and injection availability, accounting for realistic downtime, and enabling adaptive redistribution of rates when pressure responses reveal suboptimal support.

Results and Discussion

The do-nothing case (scenario A) captures only the residual tail of the existing waterflood and exhibits progressive pressure decline. Adding producers (Scenario B) accelerates drainage and lifts cumulative oil by 2020. By contrast, adding injectors (Scenario C) not only maintains pressure but, as an immiscible displacement process, also improves areal and vertical sweep efficiency—pushing oil out of poorly swept zones and thereby increasing production. Together, these results indicate that in compartmentalized North Sea settings, selective infill can add value where support is adequate, but a targeted injector program designed to close sweep shadows and balance compartmental voidage provides the strongest, most defensible IOR option for mid- to late-life operations.

This research contributes to the broader understanding of IOR applications in mature offshore fields, offering practical guidance for extending field life and bridging the transition between conventional oil production.

1. Introduction

The global petroleum industry faces many challenges as discoveries of conventional oil reservoirs are reducing, which makes it important to deal with the current reservoirs, which are experiencing a declining production rate and an increase in water production. Considering the continuous increase in energy demand worldwide, maximizing recovery from existing conventional fields has become a necessity in economic and environmental imperatives. Conventional primary recovery methods typically extract 10-20 % of the original oil in place (OOIP), leaving a huge hydrocarbons volume underground trapped in reservoirs in the pore spaces (Muggeridge et al., 2014).

IOR and EOR impact both elements of recovery (microscopic displacement efficiency and macroscopic sweep efficiency), but with differing focus (Muggeridge et al., 2014; Green & Willhite, 2018). IOR commonly refers to further optimising the primary/secondary processes without fundamentally adding a new displacement mechanism (e.g., typical measures include pressure-maintenance and waterflood optimisation [pattern realignment, injector–producer rebalancing, VRR control], conformance control [zonal isolation, profile modification], well placement and completion upgrades [infill/step-out drilling, horizontal sidetracks, smart completions], reservoir management [surveillance-driven rate/BHP control, dynamic allocation] and production optimisation [artificial lift, sand and scale management], activities that mostly impact sweep and can delay early water or gas breakthrough with limited thermal or chemical intervention [Alvarado & Manrique, 2010; Green & Willhite, 2018]). In contrast, EOR seeks to add or enhance displacement mechanisms by selectively targeting physical/chemical processes. Common mechanisms include mobility-ratio control and conformance improvement using polymers, foams, etc. to limit channeling (Sheng, 2011; Green &

Willhite, 2018); altering wettability toward more water-wet conditions with low-salinity brines and surfactants to release capillary-trapped oil (Al-Shalabi & Sepehrnoori, 2016; Sheng, 2011); lowering interfacial-tension with alkali–surfactant–polymer systems to raise capillary number (Sheng, 2011); changing viscosity/density with thermal processes or solvent co-injection to improve displacement efficiency (Green & Willhite, 2018); and near-miscible/miscible gas processes (e.g., CO₂ or rich gas above MMP) that swell oil and lower viscosity, often applied with WAG variants (Kumar et al., 2017; Song et al., 2024). In practice, IOR often precedes or is combined with EOR—IOR is used to establish pressure support and conformance, while EOR typically adds a new complementary displacement mechanism to release residual oil (Muggeridge et al., 2014; Alvarado & Manrique, 2010).

A credible assessment of these trade-offs requires a standard numerical-simulation workflow. This involves commercial reservoir simulators, built with mature and defensible PVT/EOS descriptions (black-oil/compositional as appropriate), relative-permeability and capillary-pressure functions (including hysteresis), geocellular models upscaled from the underlying geology (Reynolds,2008). This workflow typically consists of: data conditioning and history matching to reproduce past field performance; forecast modeling under realistic well/facility constraints; scenario design (injector/producer placement/pattern realignment and uncertainty/sensitivity analysis (Design of Experiments or ensemble runs) to quantify the robustness of the results. Such an approach is generally considered as industry standard since it coherently assembles disparate static/dynamic data within a physics-based, mass-balanced framework. Also, it allows explicit representation of operating limits and constraints (BHP, rates, water handling, and injection Capacity, enabling reproducible decision making via workflow, inputs, assumptions, and linking technical results to economic screening/uplift (Oliver et al., 2008; Chen et al., 2006).

2. Theoretical Background

2.1 Primary reservoir drives and production mechanisms

For a proper understanding of reservoir behavior and predicting future performance, it is necessary to know the driving mechanisms that control the behavior of fluids within reservoirs. The overall performance of oil reservoirs is largely determined by the nature of the energy, i.e., driving mechanism, available for moving the oil to the wellbore. There are basically six driving mechanisms that provide the natural energy necessary for oil recovery:

- Rock and liquid expansion drive
- Depletion drive
- Gas cap drive
- Water drive

1. For the rock and Liquid expansion drive

The oil reservoir is said to be undersaturated when it is first at a pressure that is higher than its bubble-point. Under these pressures, only oil, connate water, and rock fill the pores. As the pressure drops, the fluids expand, and the rock matrix gets tighter (grain expansion and formation compaction). This makes the pore volume smaller and pushes the fluids toward the wellbore. Because liquids and solids can only be compressed a little, pressure drops quickly with this method. The gas-oil ratio stays about the same at the bubble-point solubility. This depletion drive (rock- and fluid-expansion) is the weakest natural drive and usually only gets a small amount of the original oil in place. The recovery factor for this type of drive is 2-5 %.

2. Depletion drive

In this type of reservoir, the principal source of energy is a result of gas liberation from the crude oil and the subsequent expansion of the solution gas as the reservoir pressure is reduced. As pressure falls below the bubble-point pressure, gas bubbles are liberated within the microscopic pore spaces. Oil production by depletion drive is usually the least efficient recovery method. This is a direct result of the formation of gas saturation throughout the reservoir. Ultimate oil recovery from depletion-drive reservoirs may vary from 2% to about 5%.

3. Gas cap drive

Gas-cap-drive reservoirs can be identified by the presence of a gas cap with little or no water drive. Due to the ability of the gas cap to expand, these reservoirs are characterized by a slow decline in the reservoir pressure. The natural energy available to produce crude oil comes from the following two sources: expansion of the gas-cap gas, and expansion of the solution gas as it is liberated. The oil recovery for gas cap drive is 25-30 %.

4. Water drive

Many reservoirs are bounded on a portion or all of their peripheries by water-bearing rocks called aquifers. The water drive is the result of water moving into the pore spaces originally occupied by oil, replacing the oil and displacing it to the producing wells. Ultimate oil recovery from water-drive reservoirs around 40 %.

2.2 IOR vs EOR methods

Thomas (2008) argues that the terms EOR and IOR have been used loosely and interchangeably. IOR is a general term that implies improving oil recovery by any means. For example, operational strategies, such as infill drilling and horizontal wells, improve vertical and areal sweep, leading to an increase in oil recovery.

EOR implies a reduction in oil saturation below the residual oil saturation (Sor). Recovery of oils retained due to capillary forces (after a waterflood in light oil reservoirs), and oils that are immobile or nearly immobile due to high viscosity (heavy oils and tar sands) can be achieved only by lowering the oil saturation below S_{or} (Thomas, 2008).

Many EOR methods have been used in the past for the recovery of light and heavy oil as well as tar sands, as shown in Table 1. Thermal methods are primarily intended for heavy oils and tar sands, and non-thermal methods are normally used for light oils. Thermal methods have been tested since the 1950s and are best suited for heavy oils (10-20° API) and tar sands (≤10° API). Thermal methods such as Cyclic Steam Stimulation (CSS), steam flooding, and steam-assisted gravity Drainage (SAGD) have been highly successful in Canada, the USA, Venezuela, Indonesia, and other countries (Thomas & Farouq Ali, 2001).

Non-thermal methods, such as miscible flooding and chemical flooding, are best suited for light oils (≤100 cp) The two major objectives in non-thermal methods are lowering the interfacial tension and improving the mobility ratio (Selby et al., 1989).

Field/Location	EOR Method	Recovery Factor (%)	Additional Recovery (%)
Weyburn, Canada	CO ₂ Miscible	45–50	10–15
Daqing, China	Polymer Flooding	50–55	12–15
Kern River, USA	Steam Flooding	70–80	40–50
Karamay, China	In-Situ Combustion	62	30–40
Shengli, China	ASP Flooding	45–50	15–20
Alberta Oil Sands	SAGD	65–75	50–65

Table 1: Types of EOR Methods (Muggeridge et al., 2014)

For IOR methods composed from different methods, such as gas Injection for Pressure Maintenance, which includes the injection of gases such as nitrogen, air, and produced gas for pressure maintenance and improved displacement. Also, well Pattern and Infill Drilling is another method, and adding a new infill drilling and pattern optimization of producers and injectors can lead to improved reservoir coverage and access to bypassed oil, increasing recovery. The third method that can be considered as an IOR method is waterflooding, and according to Lyons (1996), waterflooding is the most common way to improve oil recovery, and some examples of IOR methods are shown in Table 2.

IOR Method	Main Purpose	Key Application Example
Waterflooding	Pressure maintenance, oil displacement	Sandstone reservoirs worldwide
Low Salinity/Smart Water	Wettability alteration, improved sweep	North Slope, Alaska; Shengli Field, China
Infill Drilling	Access bypassed oil, improve patterns	Mature oil fields globally
Artificial Lift	Boost wells with low pressure	ESPs/gas lift in depleted fields
Well Stimulation	Remove blockages, improve flow	Acidizing/hydraulic fracturing
Advanced Reservoir Management	Targeted recovery, operational improvement	Integrated modeling, 4D seismic

Table 2: Types of IOR Methods(Muggeridge et al., 2014)

2.3 Basic concepts of waterflooding (IOR method)

In the Norne field, which is the Norwegian field, the IOR method (waterflooding) has been used since 1997 to maintain reservoir pressure and increase the recovery of this field, and since it's an important IOR method, we will explain the theory behind the waterflooding.

The concept of mobility (λ) was first introduced by Muskat (Muskat, 1951) and represents the ratio of effective permeability of the fluid (absolute permeability K multiplied by the relative permeability kri of the fluid) to the fluid viscosity (μ i) and is a strong function of fluid saturation.

It is calculated as follows, according to equation 1:

$$\lambda_i = \frac{k k_{r_i}}{\mu_i} \tag{1}$$

The mobility ratio M describes the ratio of mobility of the displacing fluid to the mobility of the displaced fluid. Considering the case that water and oil are present, water is the displacing phase, meanwhile oil is the displaced phase, therefore the denotations w and o are respectively used in equation 2:

$$M = \frac{\lambda_{dosplacing}}{\lambda_{displaced}} = \frac{\lambda_{\omega}}{\lambda_{0}} = \frac{kr_{w}}{\mu_{w}} \frac{\mu_{o}}{kr_{w}}$$
(2)

As we can see clearly from Figure 1, the mobility ratio below 1 is favourable as it leads to a stable, piston-like displacement. If the mobility ratio is higher than 1, the displacement is unfavourable, because it is unstable and viscous fingers are very likely to develop. In other words, if the displacing fluid tends to move faster than the displaced fluid, the interface is unstable. Additionally, heterogeneity of the formation fosters the development of unstable displacement fronts. Consequently, breakthrough of water occurs much faster, which apparently leads to a decreased recovery efficiency (Muskat, 1951).

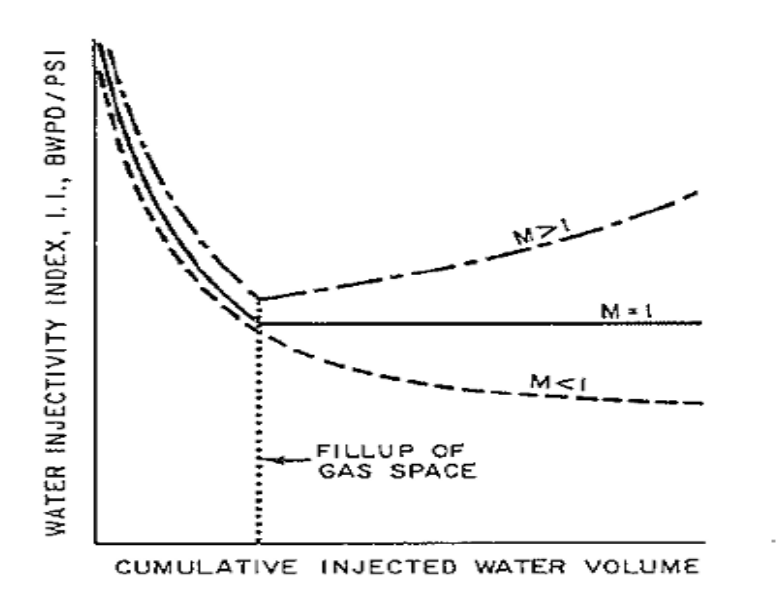


Figure 1: Water injectivity variation (Craig, 1971)

There are commonly two scales of waterflooding distinguished, which are namely the microscopic and macroscopic scales. On a microscopic scale, the interactions between injected and in-place fluids should be investigated by performing lab experiments for fluid-fluid as well as for fluid-rock interactions. From the macroscopic point the microscopic behavior is upscaled and structural set-ups and geological heterogeneities need to be considered as these features seriously impact the flow behavior (Marek & Cobb, 1997).

The efficiency of a displacement process depends on the microscopic and macroscopic displacement efficiency equation 3:

$$E = E_V * E_D \tag{3}$$

E. overall displacement efficiency

Ev. volumetric sweep efficiency / macroscopic displacement efficiency (heterogeneous)

E_D. displacement efficiency / microscopic displacement efficiency (homogeneous)

$$E_D = \frac{reservoir\ volume\ of\ oil\ mobilized}{reservoir\ volume\ of\ oil\ contacted} \tag{4}$$

The microscopic displacement is related to the displacement of oil at the pore scale and therefore, is an indicator of the effectiveness of the displacing fluid to mobilize the oil. Whereas the macroscopic displacement efficiency is related to the effectiveness of the displacing fluid to contact the reservoir in a volumetric sense. So, it measures how effectively the displacing fluid sweeps out the reservoir volume (Buckley & Leverett, 1942).

$$E_V = \frac{reservoir\ volume\ of\ oil\ contacted\ by\ displacing\ agent}{reservoir\ volume\ of\ oil\ orginally\ in\ place} \tag{5}$$

Volumetric sweep efficiency and displacement efficiency are necessary input values for the computation of cumulative oil recovery:

$$N_p = \frac{E_v E_D S_{oi} V_P}{B_o} \tag{6}$$

N_{P.} cumulative oil recovery

Soi. initial oil saturation

V_P. Pore Volume

 B_o oil formation volume factor

2.3.1 Voidage Replacement Ratio (VRR)

The voidage replacement ratio indicates the proportion of injected water required to replace the volume of oil, gas, and water produced from the tank. In other words, it is a measure of the number

of barrels of injected fluid to the number of barrels of created fluid in the reservoir. Mathematically, it can be written as the following equation (9):

$$VRR = \frac{Injected\ reservoir\ volume\ (rbbl)}{Produced\ reservoir\ volume\ (rbbl)} = \frac{B_w I_w}{B_o q_o + q_o B_g (GOR - R_S) + B_w q_w} \tag{7}$$

Bx. formation volume factor for fluid type x

Ix.. injected volume for fluid type x

qx. produced volume for fluid type x

GOR. produced Gas Oil Ratio

Rs. solution Gas Oil Ratio

We compute the voidage replacement ratio instantaneously. It is necessary to regularly adjust GORs depending on immediate volumes. Additionally, it is rather typical for the entire field to compute a cumulative VRR using GORs derived from cumulative fluids.

2.3.2 Waterflooding Patterns

Numerous different injection/production well patterns have been used. The most common ones are direct line drive, staggered line drive, five-spot, seven-spot, and nine-spot (Kimbler et al., 1964). Different pattern configurations are shown in Figure 2, in which four-, five-, seven-, and nine-spot patterns include either injectors at the corners and a producer at the center (regular) or producers at the corners and an injector at the center inverted (Rose et al., 1989).

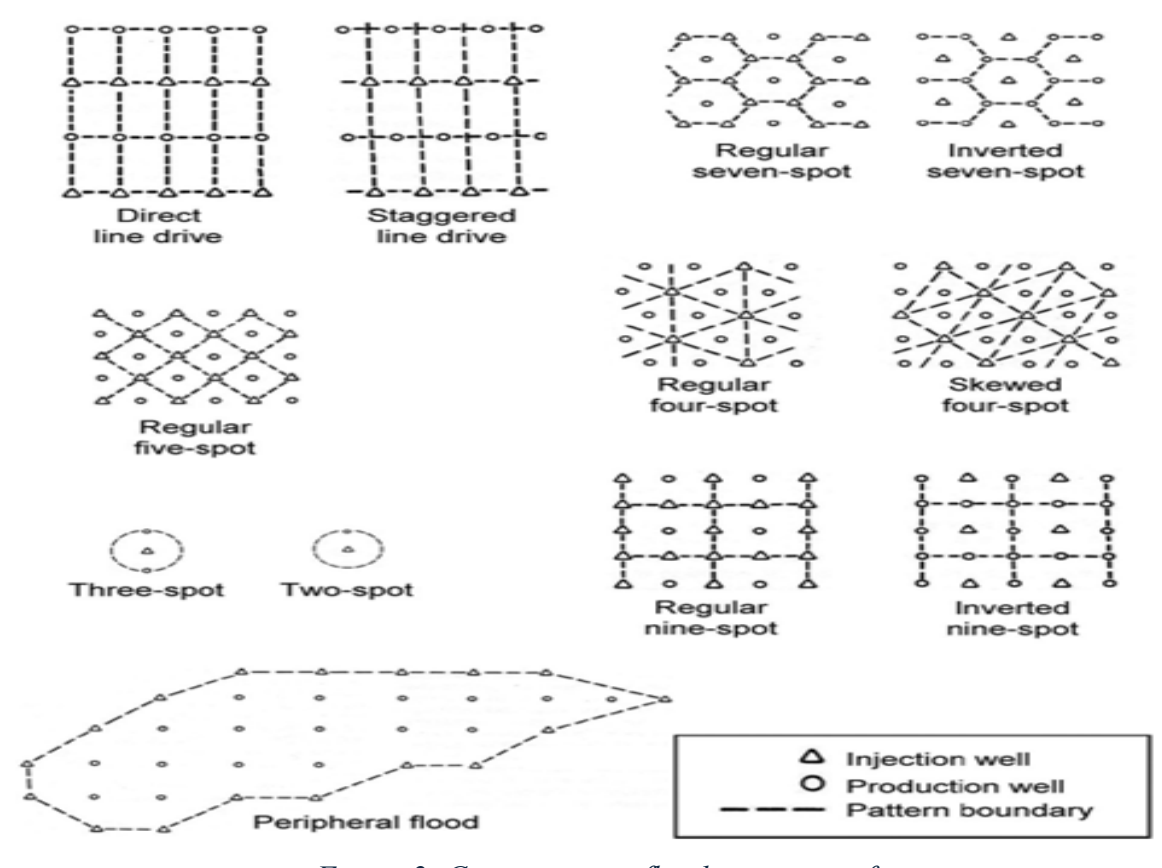


Figure 2: Common waterflood-pattern configurations

2.3.3 Fluid Properties

The physical properties of the reservoir fluids have pronounced effects on the suitability of a given reservoir for further development by water flooding. The viscosity of the crude oil is considered the most important fluid property that affects the degree of success of a waterflooding project. The oil viscosity has an important effect on determining the mobility ratio that, in turn, controls the sweep efficiency (Felsenthal et al., 1962).

2.4 Buckley Leverett Frontal Advance Calculation

The fractional flow theory, which is the basis for the frontal advance calculation, was first proposed by Buckley and Leverett in 1942. In this framework, the finite solubility of phases and the compressibility of fluids are ignored. This is because waterflooding is seen as an ideal immiscible displacement process, even though the injected water does mix with the water in the reservoir. The main thing that causes waterflooding is keeping or raising the pressure in the reservoir. The fractional flow equation, which comes from Darcy's law, shows how the displacement front moves and where it is. The produced water-oil ratio, the water saturation and fractional flow at the front, the saturation profile behind the front, and the timing of water penetration are all important things that affect how well a waterflood works (Buckley & Leverett, 1942).

The fractional flow equation is based on the general diffusivity equation, which can be expressed for a 1D case with constant density and incompressible flow as:

$$\frac{\delta q}{\delta x} + A\phi \frac{\delta S}{\delta t} = 0 \tag{8}$$

Darcy's Equation for two-phase flow:

$$q_0 = -\frac{k k_{r_0 A}}{\mu_o} (\frac{\delta Po}{\delta x} + \rho_0 g \sin \alpha)$$
 (9)

$$q_w = -\frac{kk_{r_wA}}{\mu_w} (\frac{\delta Pw}{\delta x} + \rho_w g sin \propto)$$
 (10)

Capillary Pressure: Pwoc = Po - Pw

Total flow rate: $q=q_w+q_0$

Fractional flow of water: $f_{w=\frac{q_w}{q}}$

Re-arranging the equations above leads to:

$$f_w = 1 + \frac{\frac{k k_{r_o A}}{q \mu_o} (\frac{\delta Pcow}{\delta x} - \Delta \rho g sin \propto)}{1 + \frac{k_{r_o \mu_w}}{\mu_o k_{r_w}}}$$
(11)

3. Model Characterization

3.1 Numerical Simulation and Modelling

Reservoir simulation uses both static model and dynamic model to forecast field performance and assess development options. The numerical model developed for Norne, built in Petrel, was exported to ECLIPSE 100, SLB and used for numerical simulations.

In the Static modelling (Petrel), the seismic, well logs, and core were used to constrain the structural framework, facies architecture, and petrophysical characteristics (porosity, permeability, net-to-gross, and Swirr). Quality control was based on well-to-seismic correlations, fault sealing/connectivity verification, and upscaling validation (log-scale and model-scale properties).

For the Dynamic modelling (ECLIPSE), the Petrel static model was integrated with black-oil PVT, relative-permeability, and capillary-pressure functions (SCAL), aquifer/edge-water representation where identified, and historical well controls. Fault transmissibility multipliers and vertical anisotropy (kv/kh) were tuned to match the observed connectivity trend. Outputs include field-level KPIs (field oil production total, field water production total, pressure) and map-based diagnostics to evaluate sweep. By coupling the static and dynamic models, we can quantify how water injection and well placement influence pressure support, sweep efficiency, and recovery in a mature, compartmentalised reservoir.

3.2 Static Model

The Norne field is a notable oil and gas reservoir situated in the Norwegian Sea, around 85 kilometres north of the Heidrun field Figure 3. The field is in Jurassic sandstone strata, with oil mostly present in the Ile and Tofte formations and gas in the Garn formation, at a depth of around 2,500 meters below sea level.



Figure 3: Norne field Location (Norwegian Petroleum, 2024)

The static model was built in 2004 using software such as Petrel and is based on interpreted 3D seismic data, wireline logs, and core measurements to define horizons, faults, lithology, and properties such as porosity and permeability as shown in Figure 4, with a total number of cells of 46*112*22, DX ~80-100 m, DY ~80-100, and stratified into 22 geological layers and partitioned into 16 FIP regions for volumetric control. Zonation is based on reservoir formation and stratigraphy: Garn (top), Ile, Tofte, Tilje (base), with the not formation acting as a seal between upper and lower reservoir sections. Faults are represented as transmissibility multipliers in the

model, and are described by detailed seismic cross-sections. This accounts for their impact on fluid flow and compartmentalization.

The static model also defines petrophysical properties distributed across the grid. Average porosity in the reservoir ranges from 19–26%, permeability from 187 to 1,087 mD in hydrocarbon zones, and water saturation between 20–36%. Geological features such as main blocks, fault planes, and cap rock boundaries are mapped in detail using horizon interpretation from seismic cubes.

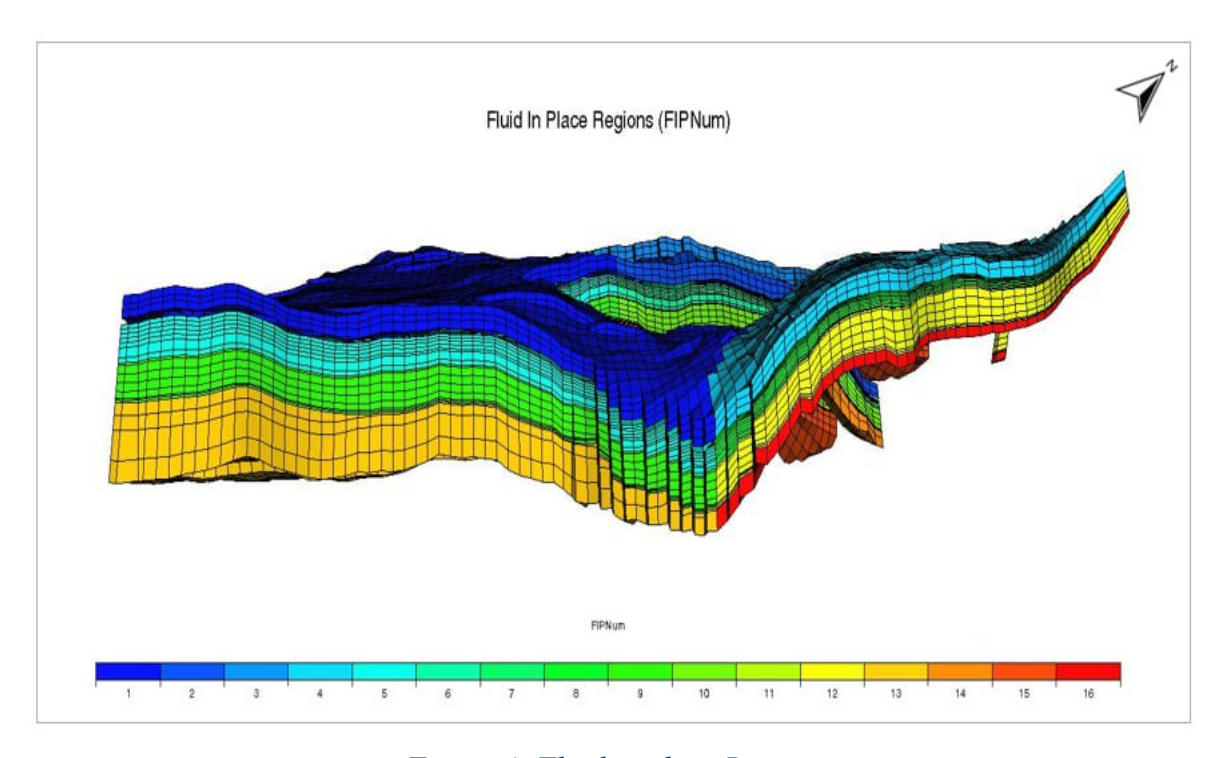


Figure 4: Fluid in place Regions

3.2.1 Reservoir Description

The Norne Field reservoir is characterized by several key properties that define its geological and production potential. These parameters, shown in the table below (Table 3), highlight the Norne field's significant hydrocarbon resources and its production history.

Reservoir Properties	Value
Depth (m)	2578-2802
Thickness (m)	224
Mean Porosity (-)	0.25
Mean Absolute Permeability (mD)	900
Average Irreducible water saturation (-)	0.19
Net to Gross (-)	0.7-1
Intial Pressure (Bar)	272

Table 3:Norne Field Key Properties

Figure 5 represents a stratigraphic representation of the Norne field, detailing its geological formations, depositional environments, and reservoir properties. The column spans the Lower to Middle Jurassic periods, specifically from the Pliensbachian to Callovian ages. It has two primary groups: the Båt Group (Tilje and Tofte formations) and the Fangst Group (Ile and Garn forms). Each formation is subdivided into units (e.g., Tilje 1–4 and Tofte 1–2) according to variations in depositional environments and reservoir quality. The Båt Group has a permeability range of 100 to 2500 mD, whereas the Fangst Group displays a range of 10 to 1000 mD. The average porosity ranges from 18% to 25%, indicating favourable conditions for hydrocarbon storage. The grain sizes vary from very fine (0.062 mm) to fine sandstones (0.177 mm), characteristic of high-quality reservoirs. The unit thicknesses vary from 9 to 35 meters, significantly increasing the reservoir's capacity. The Garn Formation has excellent reservoir quality due to its high permeability and porosity. The Tilje Formation has more complex depositional settings, including bay deposits and lower shoreface transitions. This

stratigraphic column provides critical insights into the Norne field's reservoir heterogeneity, helping in understanding fluid flow dynamics and optimizing hydrocarbon recovery strategies.

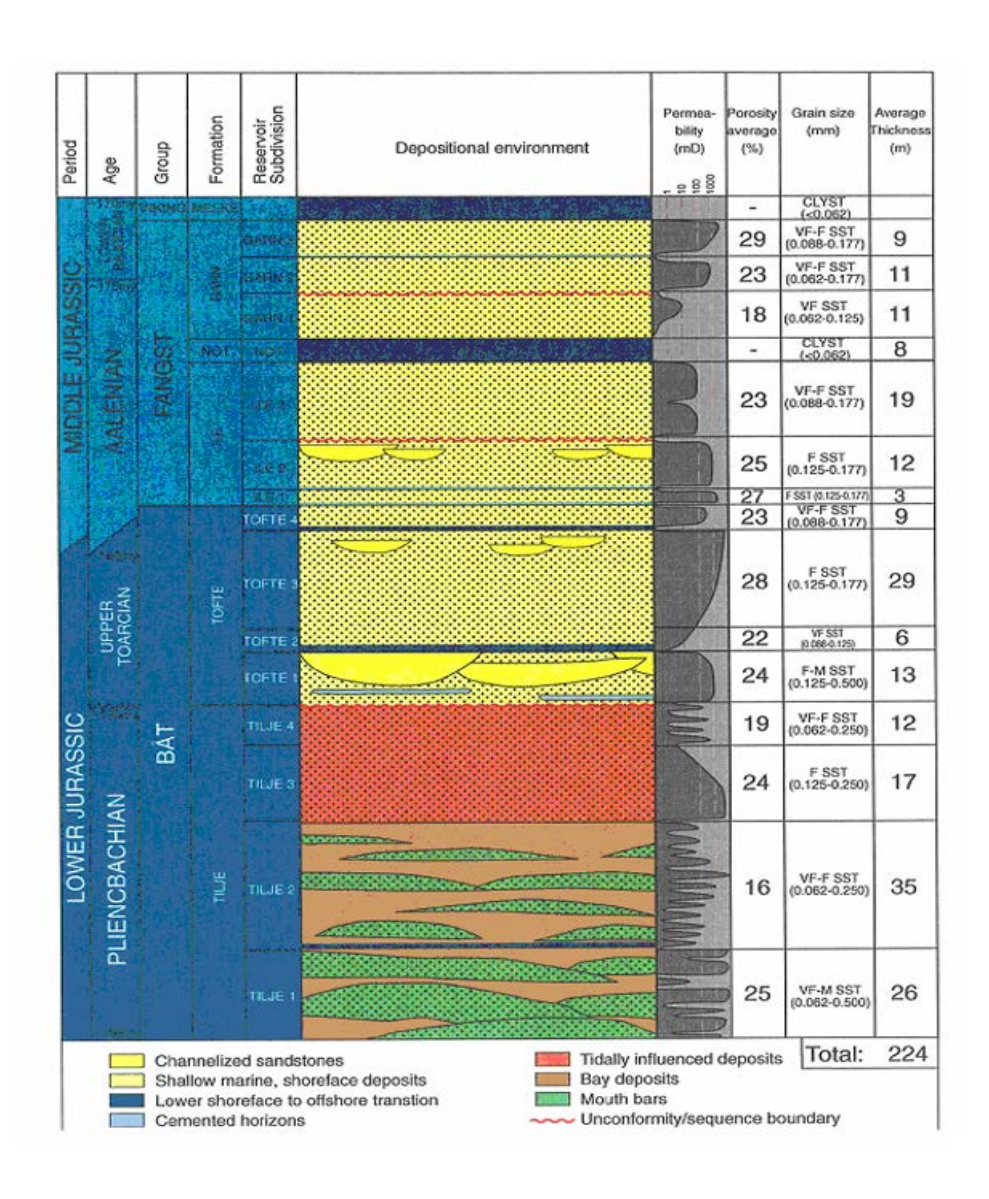


Figure 5: Stratigraphical sub-division of Norne Reservoir

3.3 Dynamic Model

3.3.1 Dynamic model construction

The Norne Field dynamic reservoir model employs a three-dimensional grid, typically 46 × 112 × 22 with approximately 44,000–45,000 active cells, mirroring the static model spatially. The simulation model is divided physically into upper and lower reservoir zones (3 layers upper, 18 layers lower), separated by the NOT formation shale barrier which is considered as a layer 4. The model operates using a black oil approach, simulating multiphase flow (oil, water, gas) through porous media. Dynamic input parameters include relative permeability, capillary pressure, initial reservoir pressures, fluid properties (PVT), and historical well events for calibration. Model calibration is achieved using history matching, aligning simulated production profiles (oil, water, gas rates, pressures) with observed field data from 22 producers and 9 injectors between 1997 and 2006. Fault transmissibility multipliers are incorporated to account for compartmentalization and fluid communication across fault blocks. Workflow often uses both manual and automated history matching (e.g., Ensemble Kalman Filter, mixture of experts machine learning, pilot point methods) to update key properties like permeability and porosity.

3.3.2 Reservoir Production and Pressure History

The Norne field was produced by water injection as a drive mechanism. Gas injection ceased in 2006, and all gas is exported. The initial pressure of the reservoir was 272 bars, and the production started by well D-1H, and to maintain the pressure, the injection started by well C-4H. The development plan of the Norne field continued by adding new producers and injectors up to November 2006; the total number of production wells is 23, and 11 injectors. The production from the field reached its maximum in 2001, and the production started to decline, reaching 11000 Sm3/day as shown in the Figure 6. In Figure 7, at the end of history in 2006, we can see clearly a mismatch between FOPTH (field oil production total history) and FOPT (Field oil production total), and the model was pessimistic.

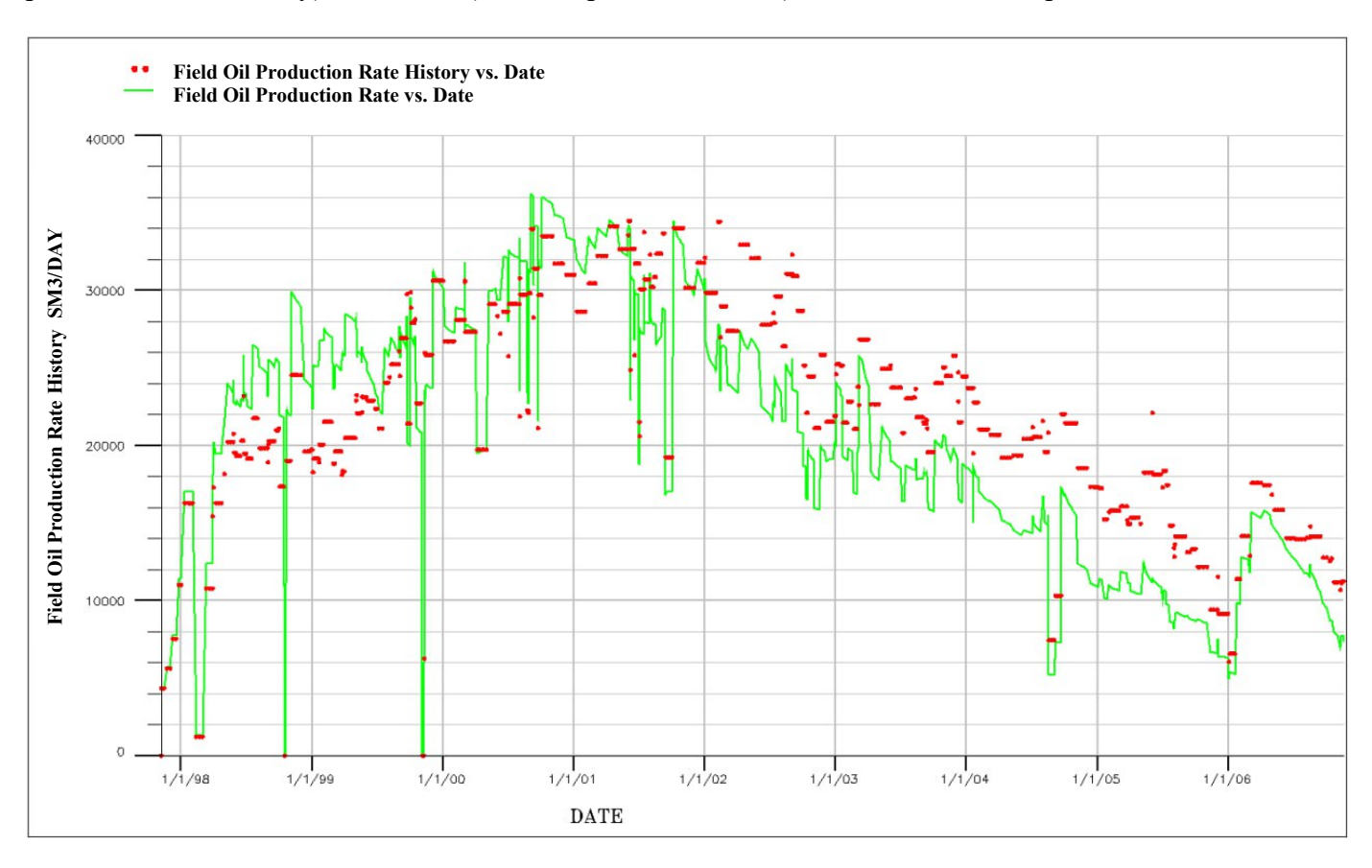


Figure 6: field oil production rate (Model vs History)

The graph in November 2006, the total oil produced was 72.4 million Sm³, with a recovery factor of 45%.

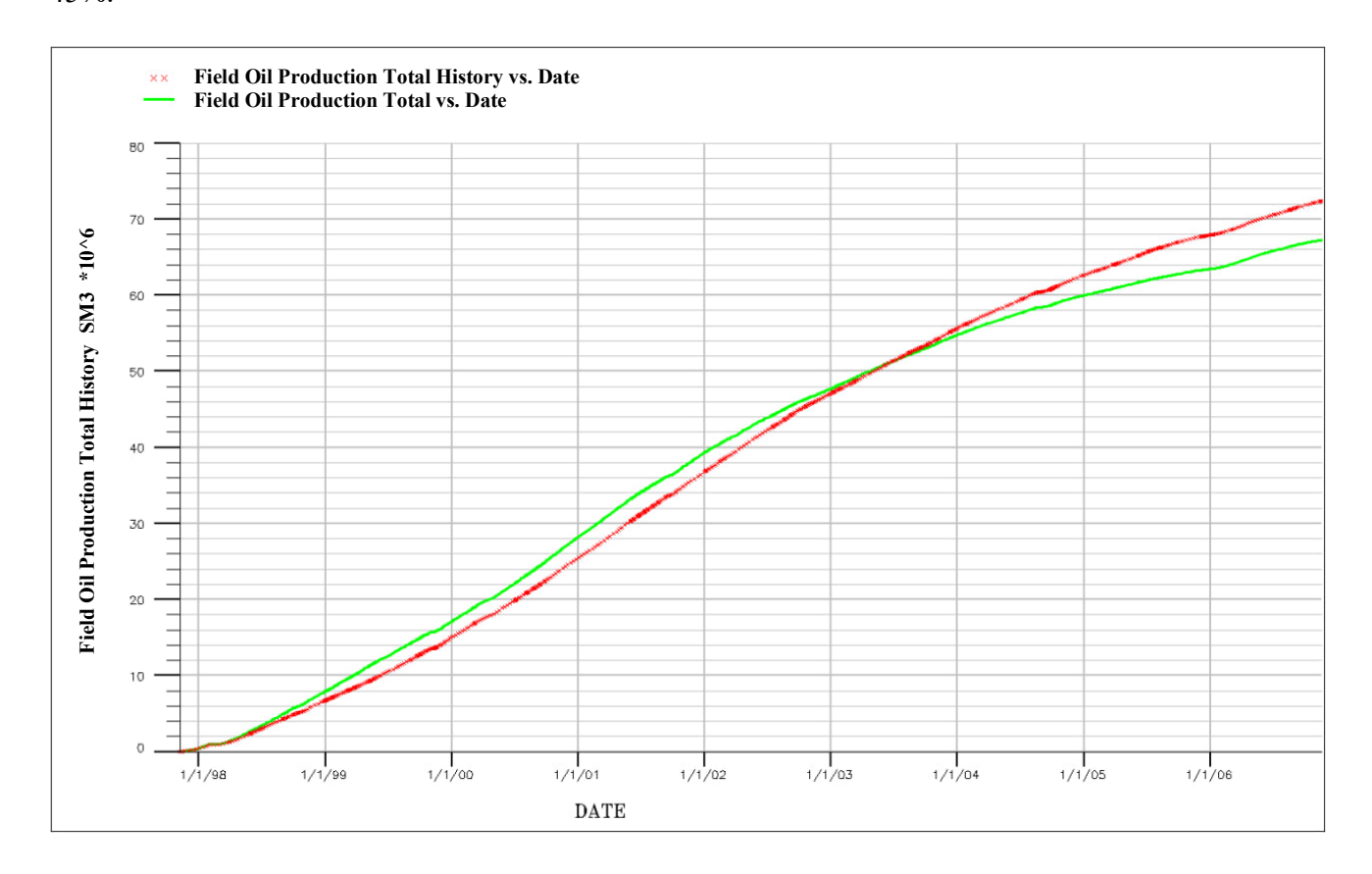


Figure 7: Total field oil production rate (Model vs History)

In Figure 8, during the first two years, there was no production of water. However, after 2000–2001, water rates started to increase progressively, reaching around 10,000–12,000 Sm³/day by 2003 and continuing upward to 18,000–20,000 Sm³/day by 2006. This clear upward trend in water production corresponds to waterfront advancement and breakthrough in producing wells. The simulated model is able to match the early breakthrough in 1999.

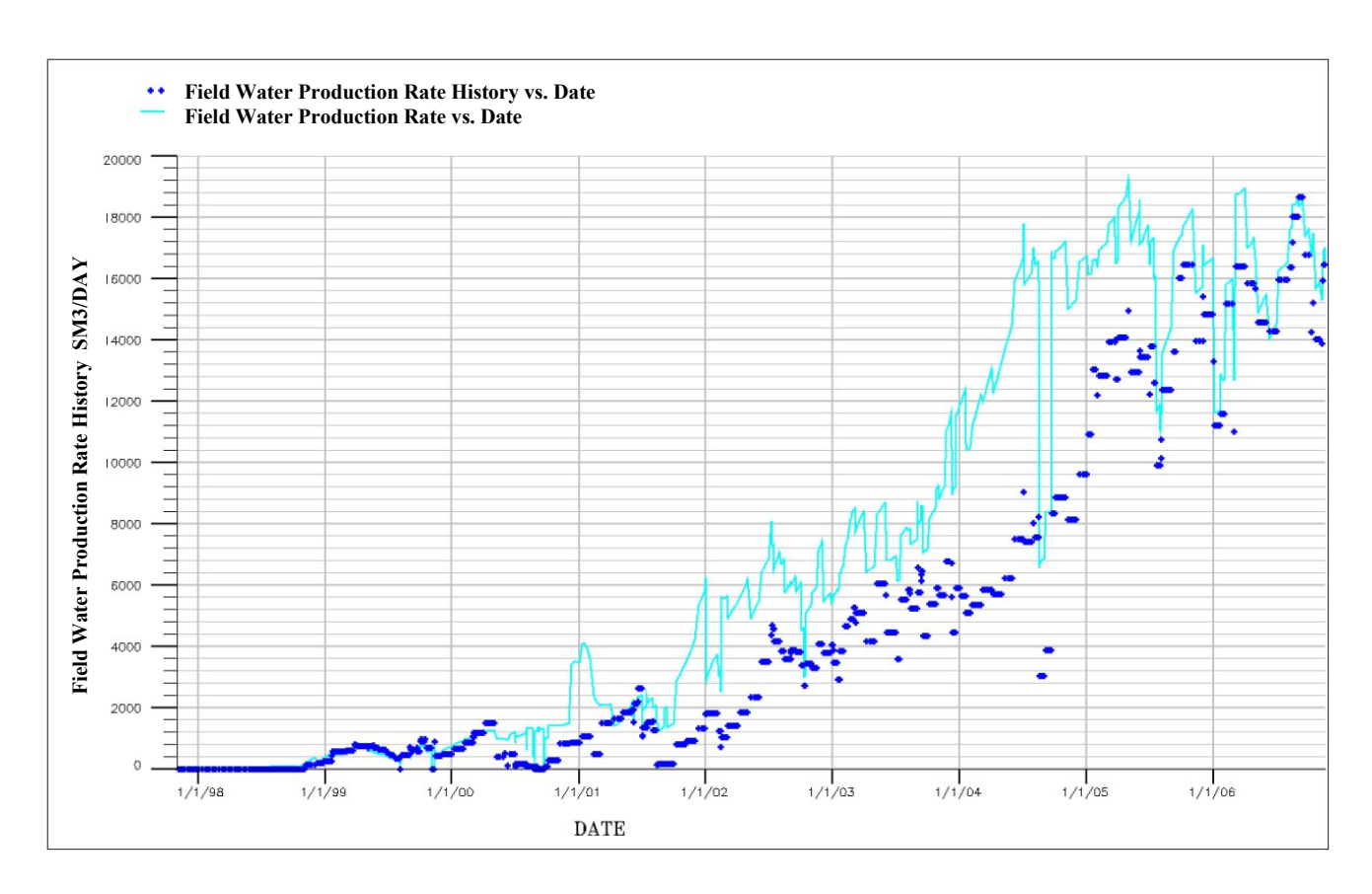


Figure 8: Field water production rate (Model vs History)

The water injection started in July 1998 with the well C-1H at a rate of 5000 Sm3/day. The injection rate of water increased progressively to reach its maximum of 50000 Sm3/day in 2001. After that, it fluctuated, and these fluctuations were due to the use of these wells to inject gas and then decreased to around 20000Sm3/day in 2006. Regarding the match between FWIR (field water injection rate) and FWIRH (field water injection rate history), the model shows a good match as shown in Figure 9.

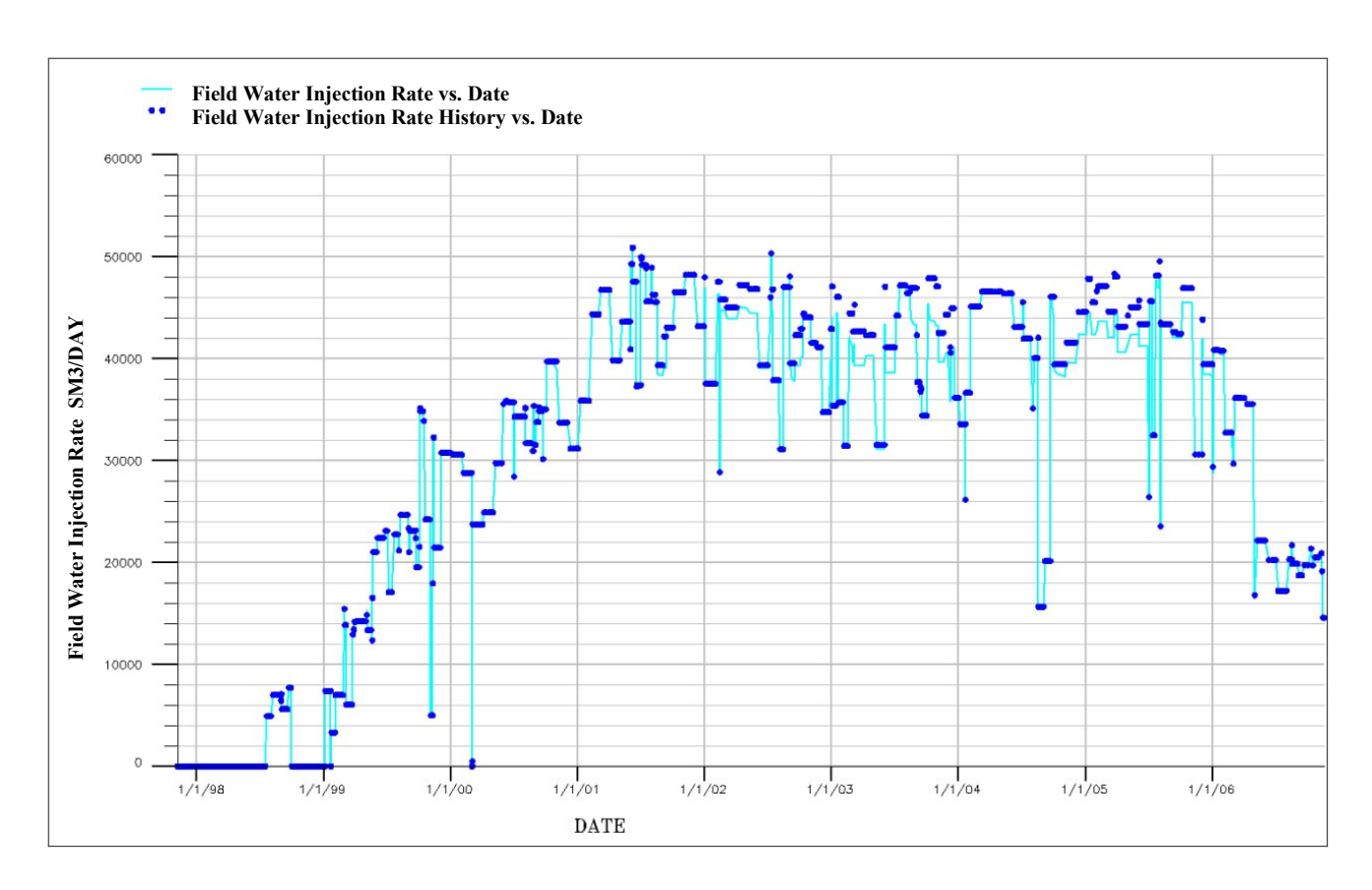


Figure 9: Field water injection rate (Model vs History)

In Figure 10, the model shows a good match between FGPR (field gas production rate) and FGPRH (field gas production rate history). The maximum production of gas reached 66 million Sm3/day in 2001 and similarly to oil production the gas production declined to 20 million Sm3/day at the end of history. In Figure 11, the model showed a good match between the FGIR (field gas injected rate) and FGIRH (field gas injection rate historical).

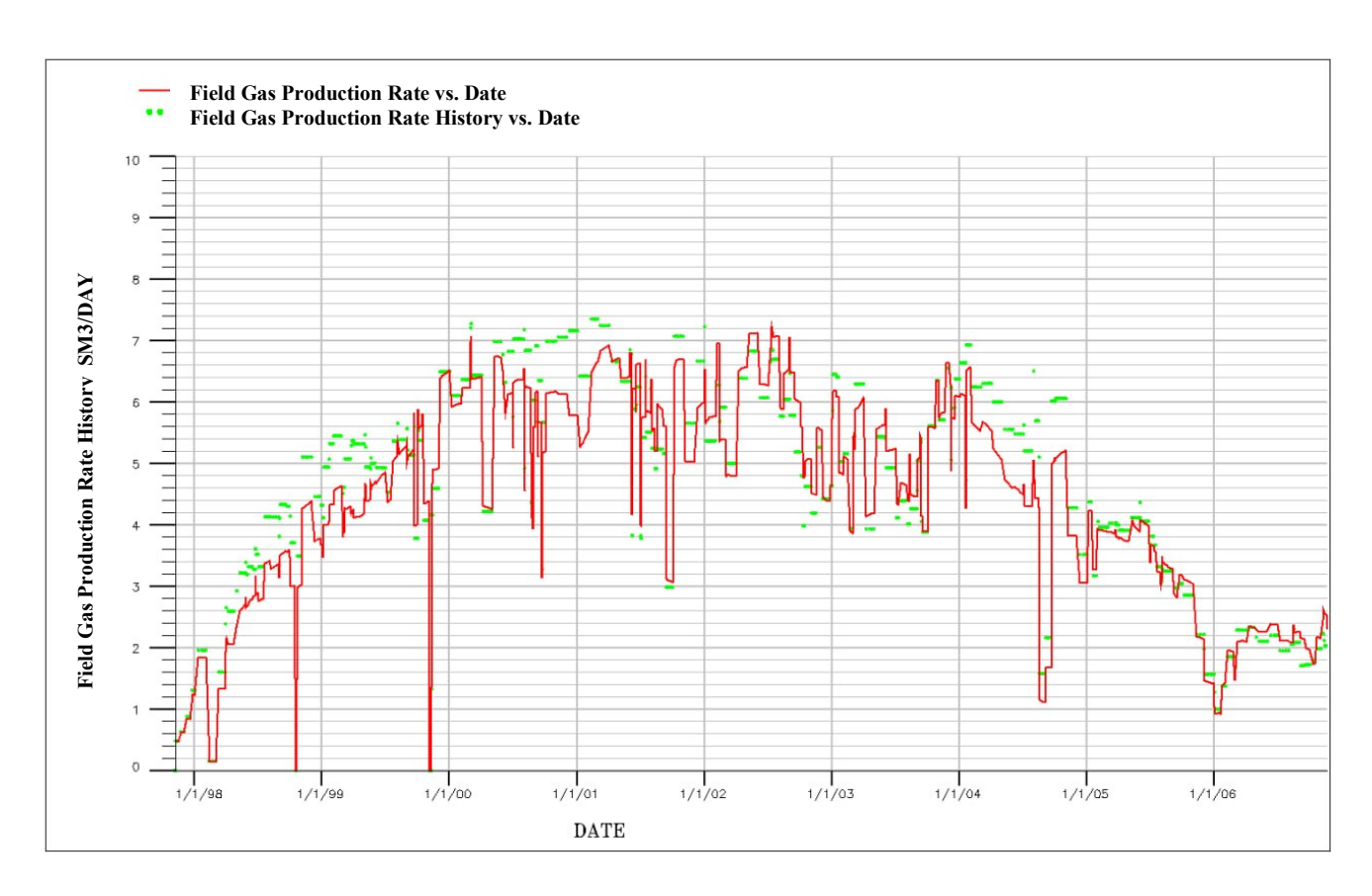


Figure 10: Field gas production rate (Model vs History)

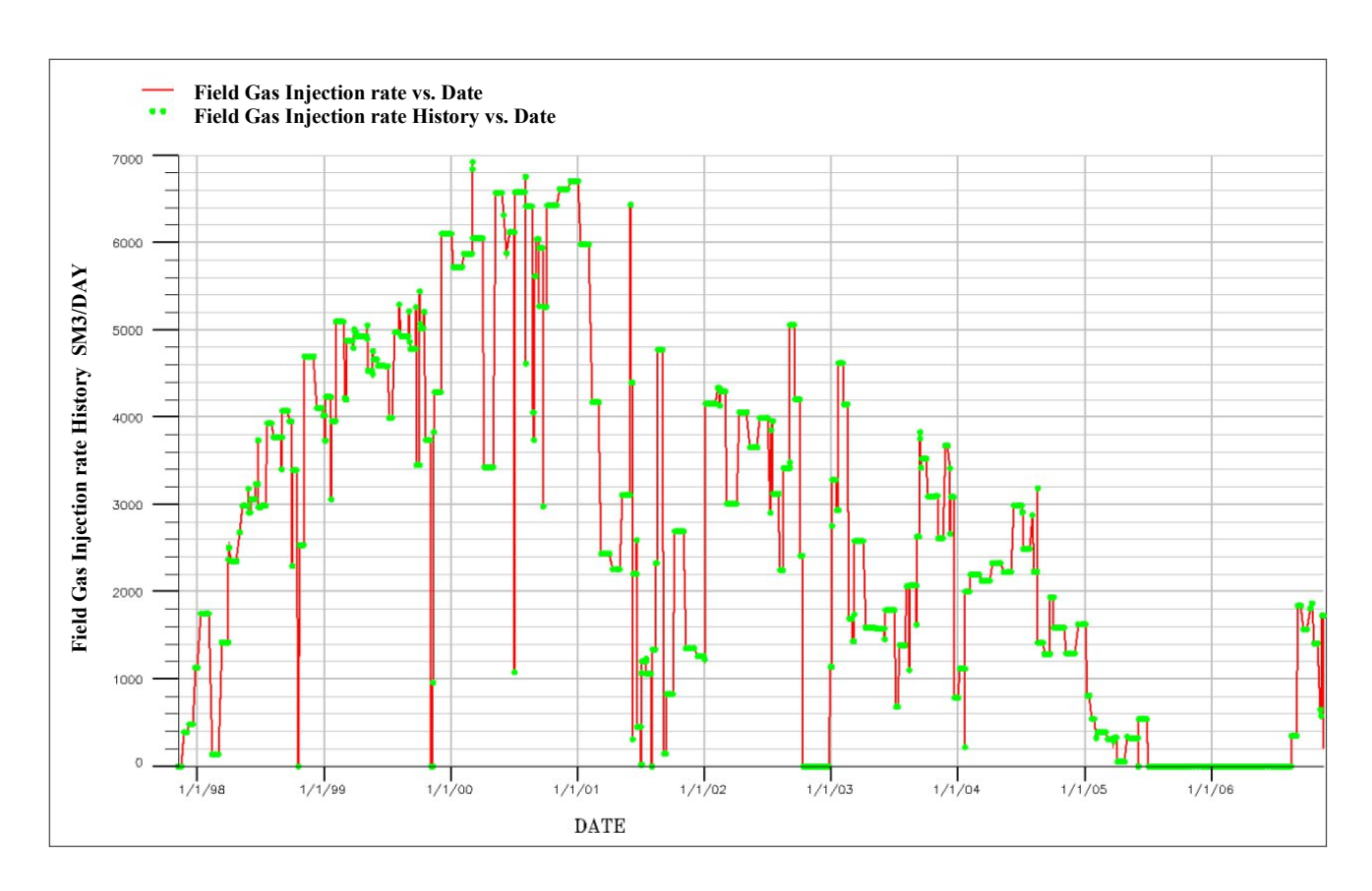


Figure 11: Field gas injection rate (Model vs History)

Table 4 ,below summarizes the following information: the original oil in place was assessed at approximately 160 million standard cubic meters, while the original gas in place was estimated at around 27 billion standard cubic meters .From 1997 to 2006, we can calculate the recovery factor for both oil and gas, which are 45 % and 56 % respectively.

	Production and Injection History	Value
Oil	OOIP	160 Million sm3
	Total Oil Production (1997-2006)	72.4 Million sm3
	GOIP	27 Billion sm3
Gas	Total Gas Production (1997-2006)	15.3 Billion sm3
	Total Gas Injected (1997-2006)	8.7 Billion sm3
Water	Total Production water	16 Million sm3
	Total Injected water	103.8 Million sm3

Table 4:Reservoir HOIP and Production

4. Forecast Scenarios: results and Discussion

This section presents and interprets the forecast outcomes of the three development scenarios, starting from the history-consistent state at end-2006. Comparisons focus on field-level KPIs (average reservoir pressure, oil/water/gas rates, and cumulative volumes) and on spatial diagnostics from oil-saturation maps. Unless stated otherwise, all scenarios honor the same operating and facility envelope (producer/injector BHP limits, cut-offs, and a field water-injection capacity cap).

4.1 Scenario A: Do nothing

In the Norne dynamic model, a do-nothing forecast was run from the end of history (November 2006) to January 2020. 11 producers and 5 injectors were kept active, using each well's most recent performance as the baseline. Producer controls: oil-rate targets were set to the latest measured oil rates, the maximum liquid rate was limited to 8,000 Sm3/day, the minimum bottom-hole pressure to 60 bar, and cutoffs were applied at 90% water cut and 1,000 Sm3/Sm3 GOR. Injector controls: recent average injection rates (three-month mean) were used, and the maximum allowable bottomhole pressure was 300 bar, subject to a fieldwide injection capacity of 42,000 Sm3/day. Figure 12 shows the reservoir porosity map with drilled wells (producers and injectors) in the Norne field.

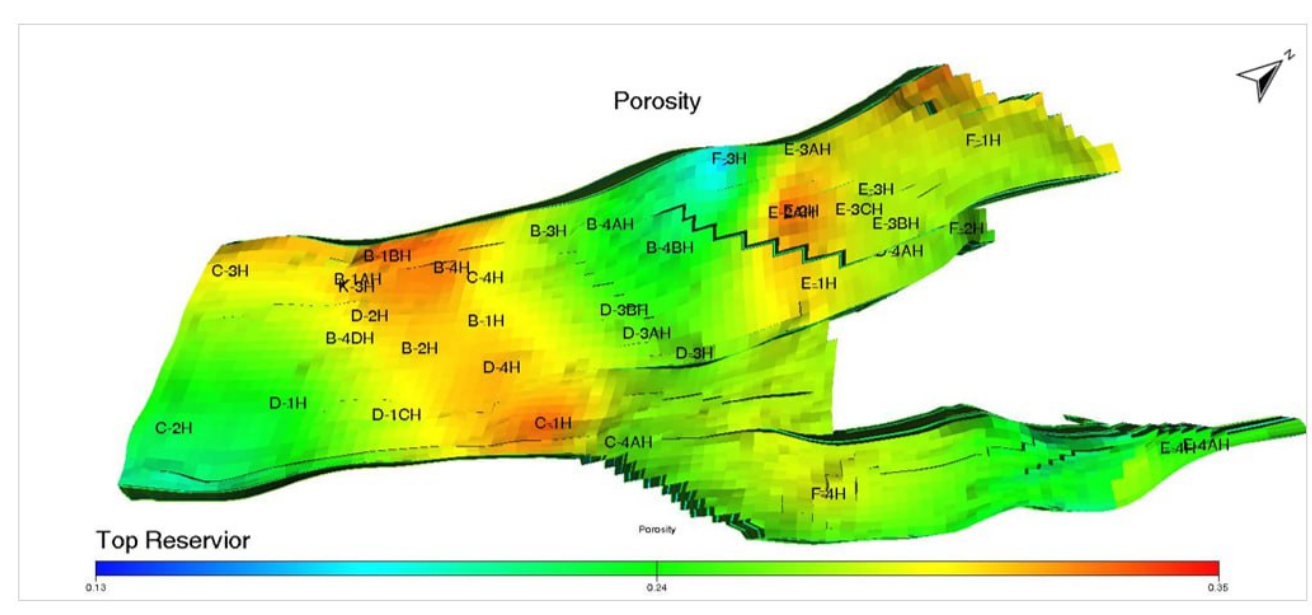


Figure 12:Location of existing wells

Figure 13 shows reservoir pressure during history and the subsequent forecast. The initial reservoir pressure was approximately 272 bar; following production, it declined rapidly, but injection-maintained reservoir pressure throughout the forecast period.

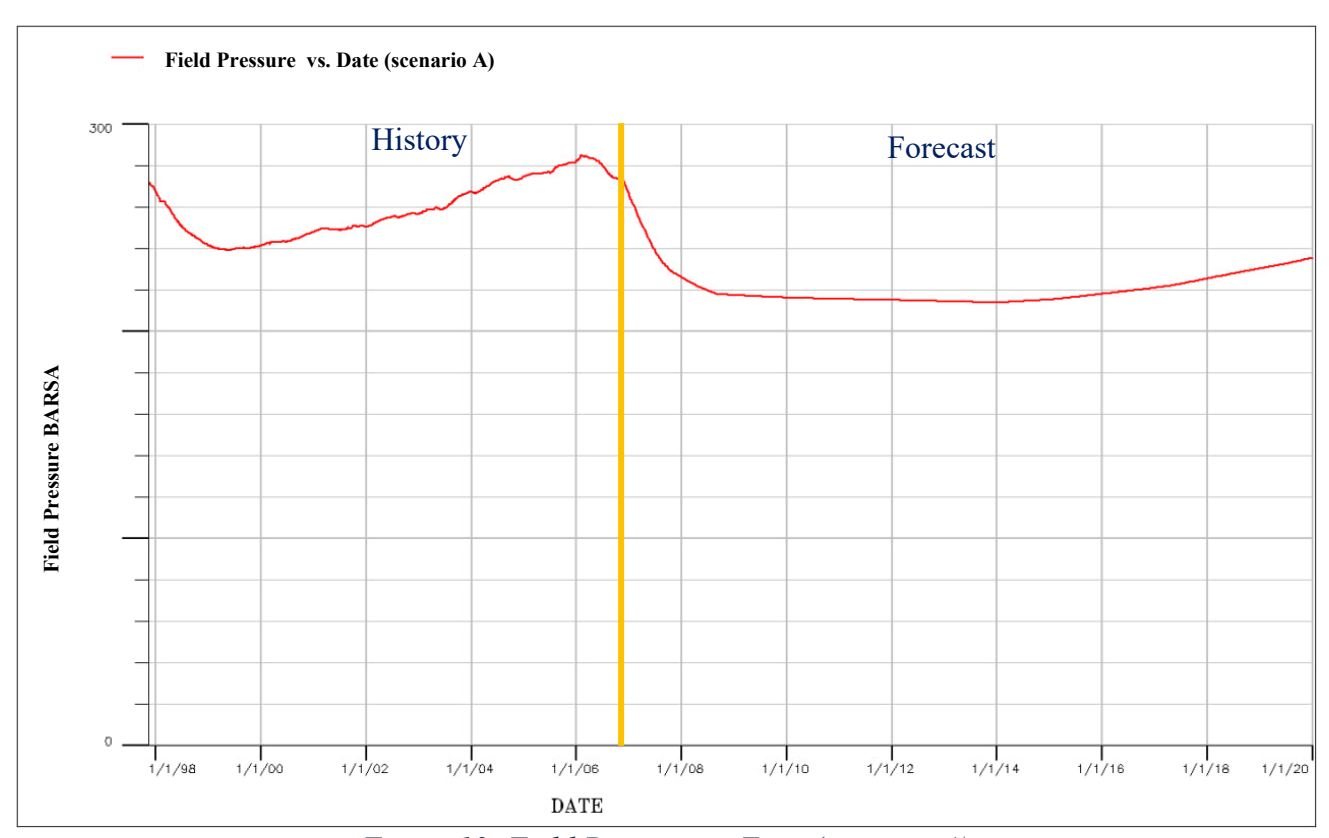


Figure 13: Field Pressure vs Time (scenario A)

Figure 14 shows the field oil production rate (FOPR) for the full history and the forecast. The field exhibits an overall decline; a temporary increase of roughly 9,000 Sm3/d occurred in January 2006, driven mainly by the start-up of new wells B-1BH and D-3BH, after which the declining trend resumed.

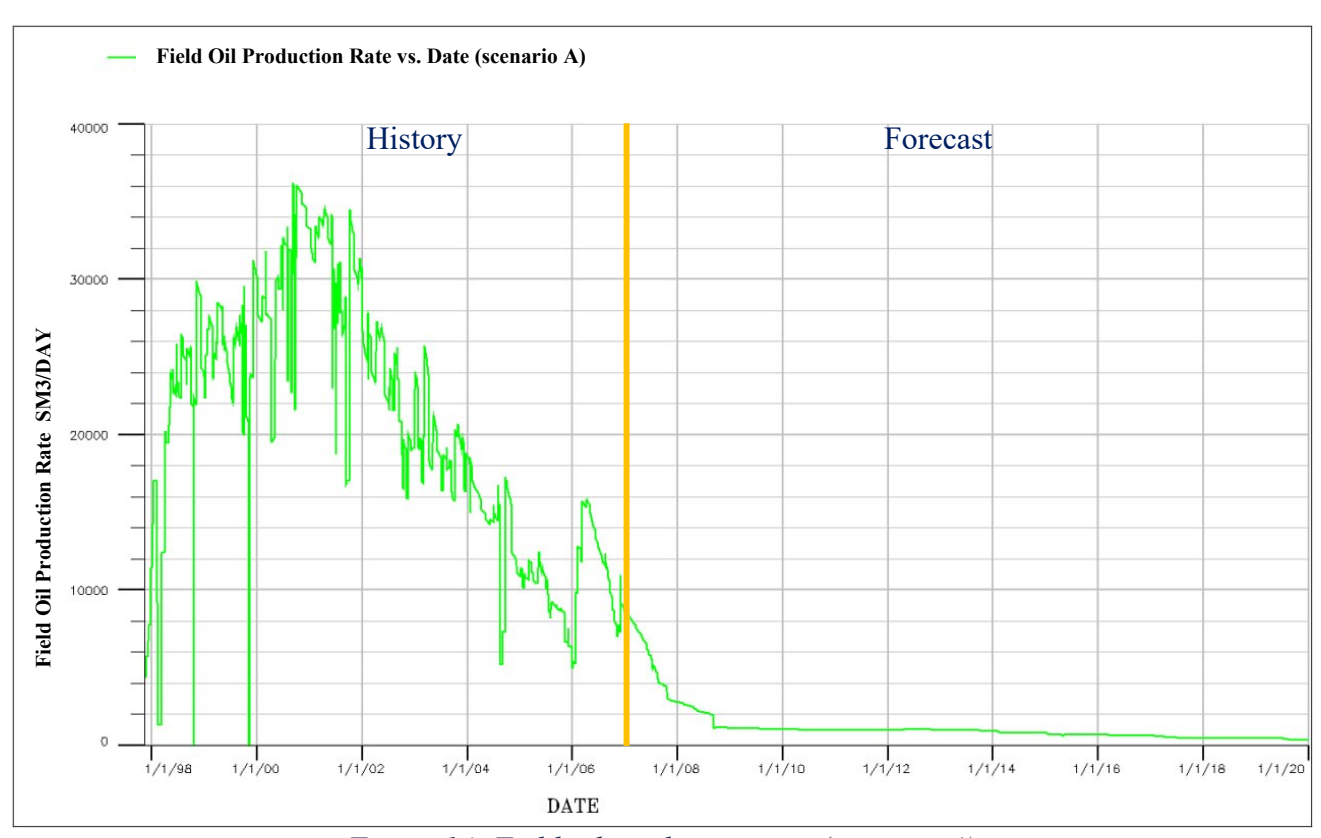


Figure 14: Field oil production rate (scenario A)

Figure 15 shows the cumulative field oil production (FOPT); the forecast predicts a total recovery of approximately 73.3×10^6 Sm3 by January 2020, corresponding to a recovery factor (RF) of 45.8% of original oil in place (OOIP).

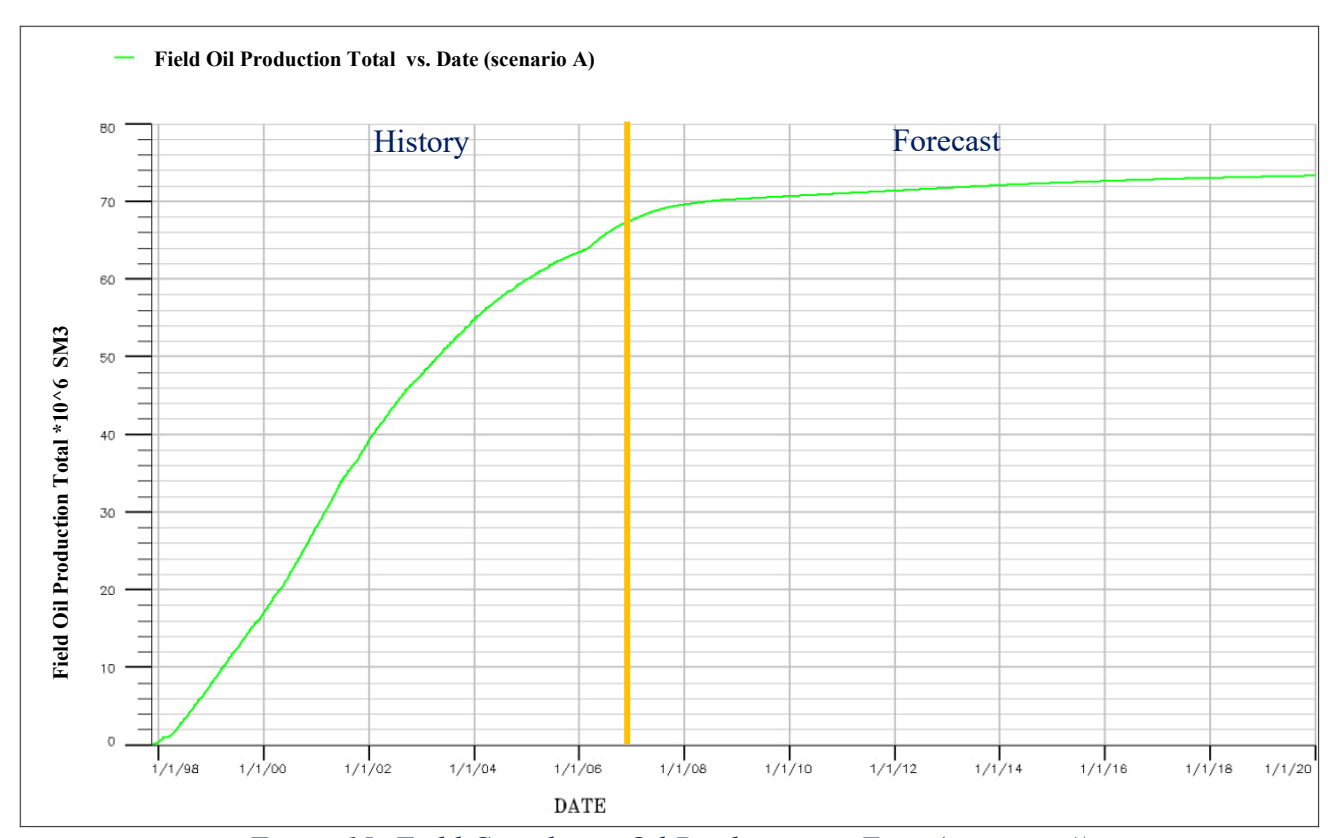


Figure 15: Field Cumulative Oil Production vs Time (scenario A)

Figure 16 shows the field gas production rate (FGPR), which follows the same to the oil rate; gas production peaked in 2001–2002 at approximately 7×10^6 Sm3/d.

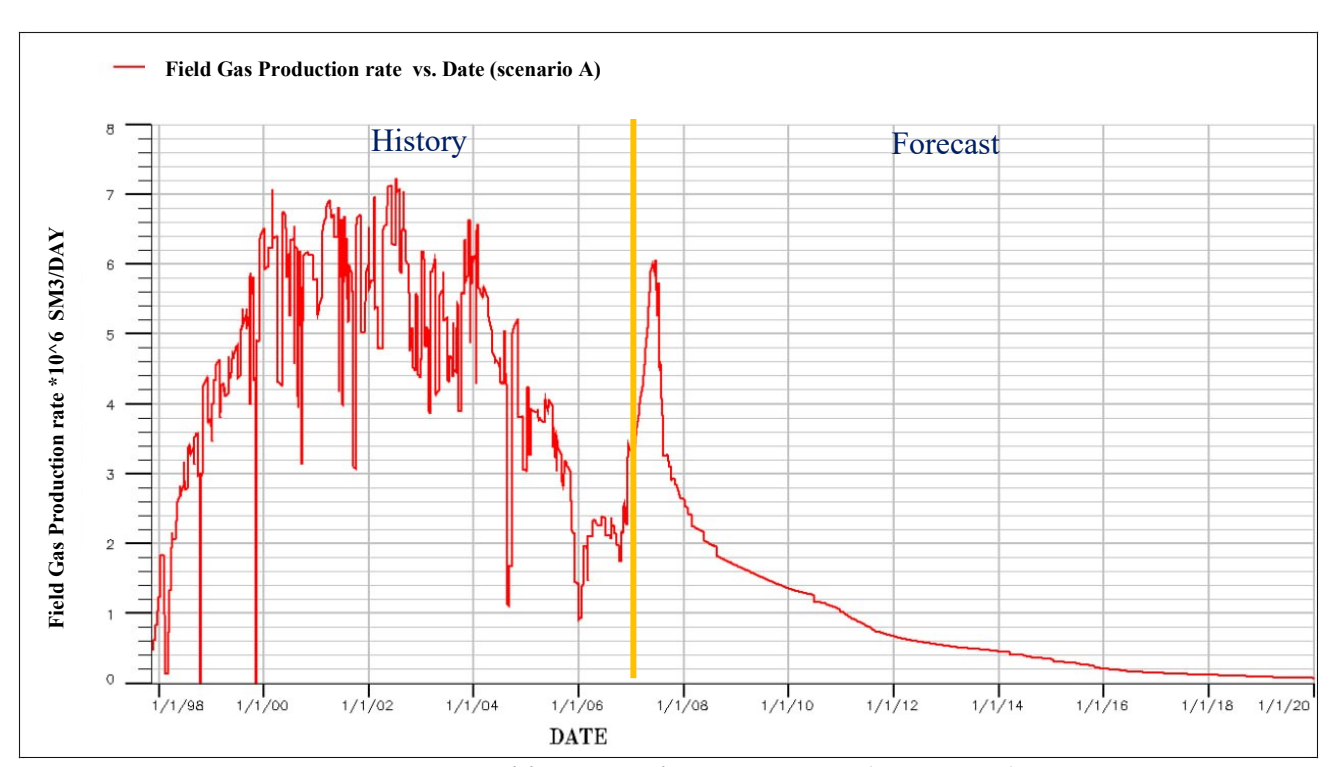


Figure 16: Field Gas Production vs Time (scenario A)

Figure 17 shows cumulative field gas production (FGPT); the forecast indicates it will reach approximately 17.6×10^9 Sm3 by January 2020. The recovery factor for gas production is 65 %.

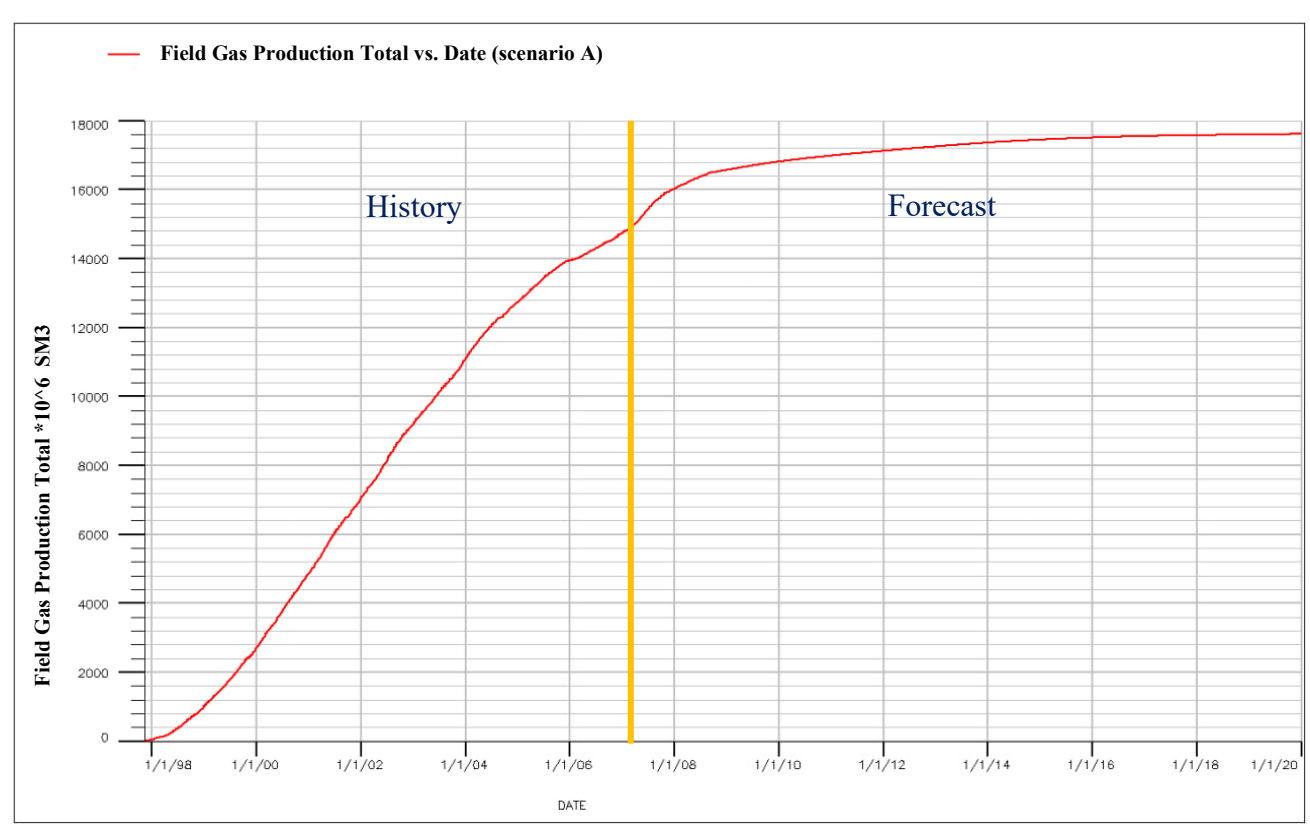


Figure 17: Field Cumulative Gas Production vs Time (scenario A)

Figure 18 shows the field water production rate (FWPR). Water breakthrough occurred in 1998, and water production steadily increased thereafter, reaching about 19,000 Sm3/day. The rising water cut negatively impacts oil production, so mechanical water-shutoff interventions were executed to preserve oil rates. Figure 19 shows cumulative field water production (FWPT), which reaches approximately 49.2 × 10⁶ Sm3 by the end of field life in January 2020. Figure 20 shows field water injection rates; injection increased over the field life to a maximum of about 50,000 Sm3/d, and at the beginning of 2006, injection was reduced as the pressure decline eased following the drop in oil production.

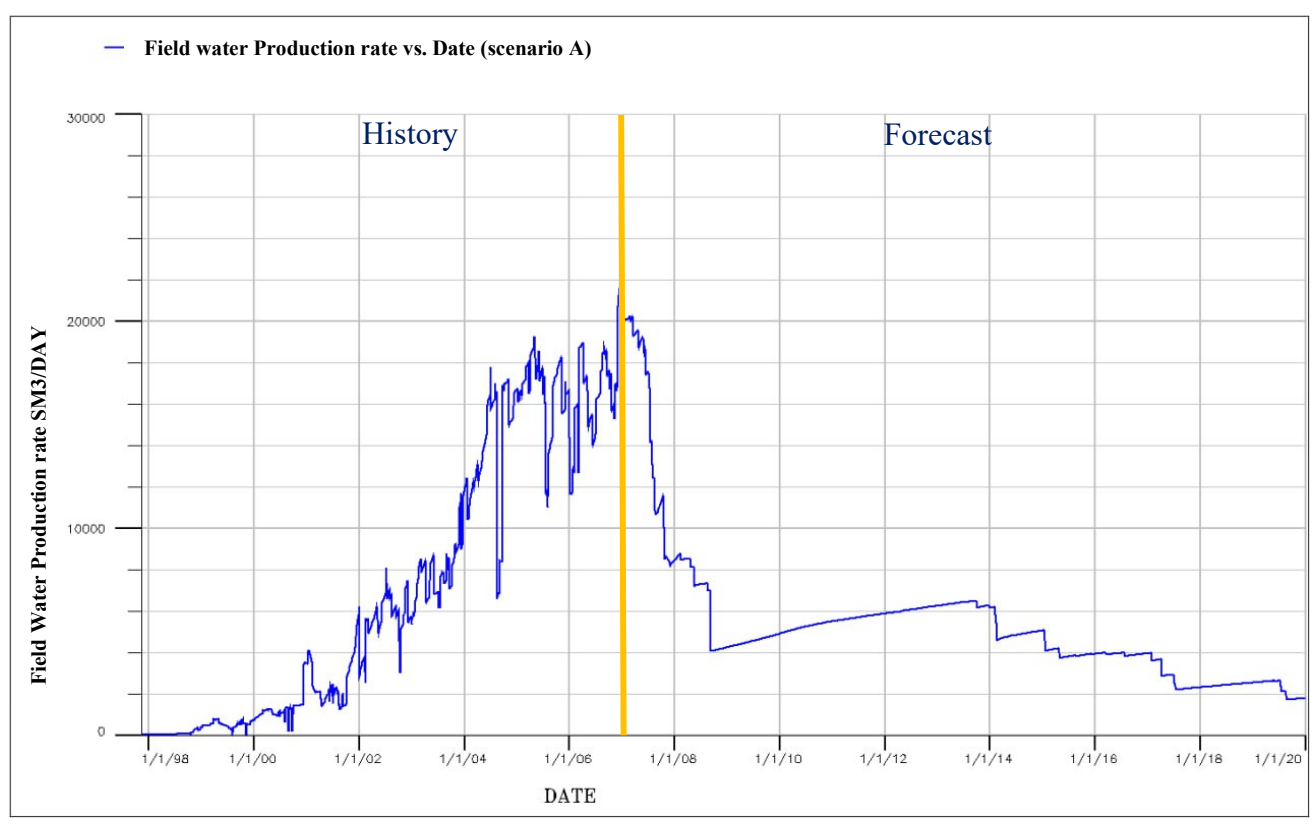


Figure 18: Field water production rate vs Time (scenario A)

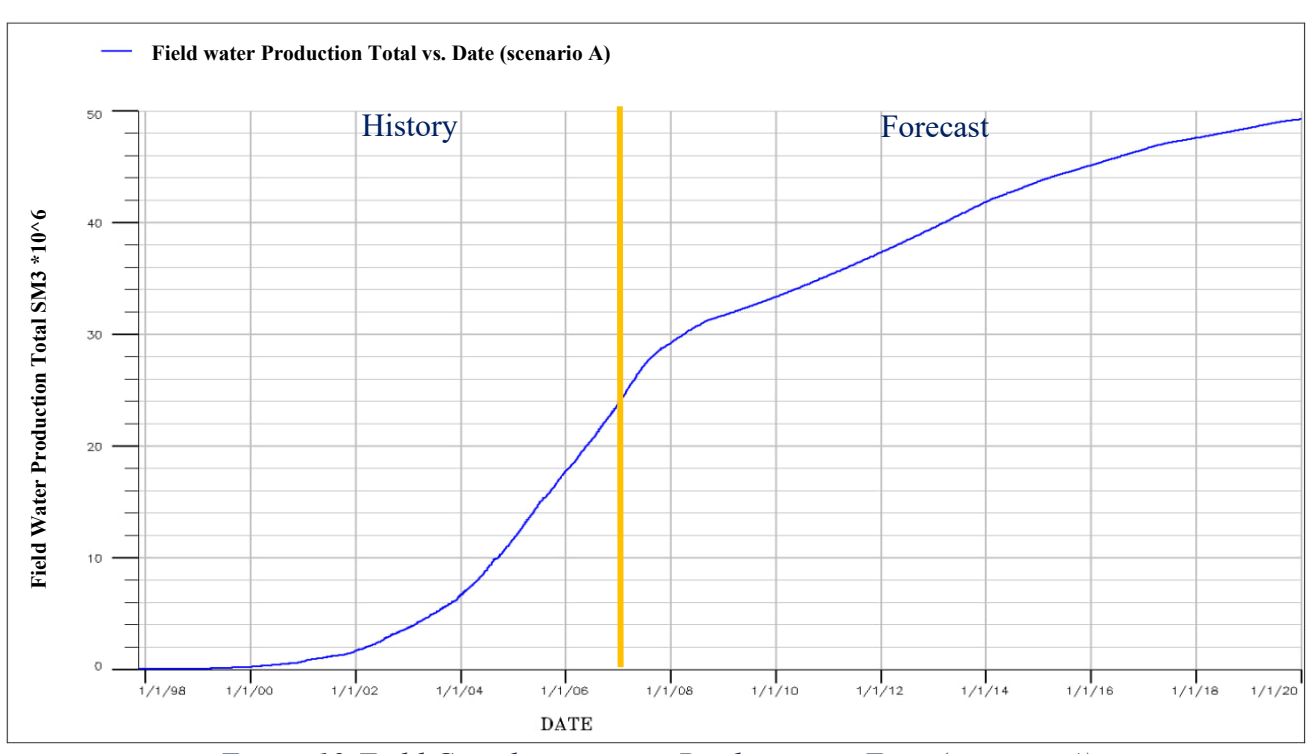


Figure 19:Field Cumulative water Production vs Time (scenario A)

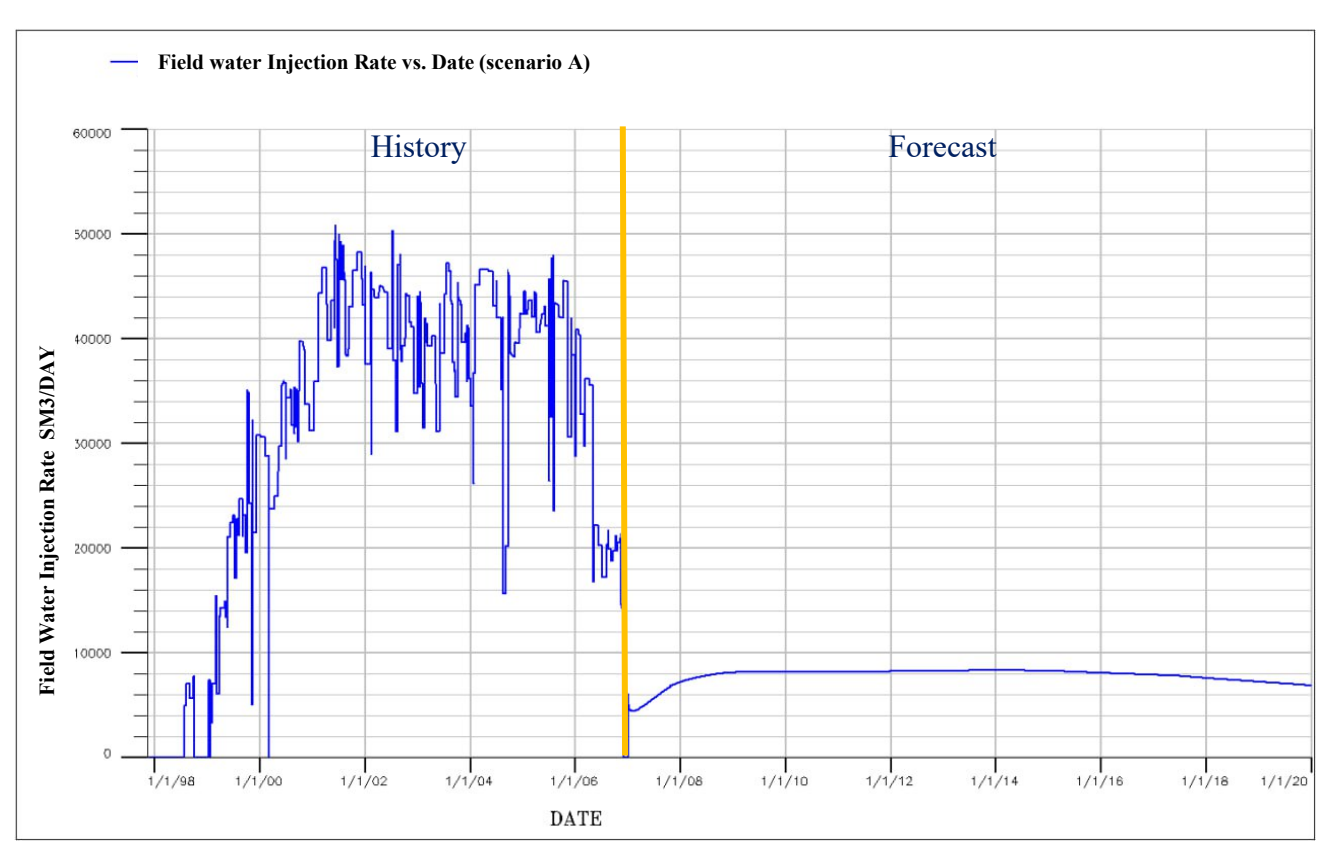


Figure 20: Field water injection rate vs Time (scenario A)

4.2 Scenario B: Scenario A (Do Nothing)+ new production wells

In this scenario, new production wells were planned to improve oil recovery. The dynamic model was used to forecast reservoir performance with added producers. A sensitivity study tested multiple candidate locations to maximise incremental oil recovery. Location selection criteria included: high oil saturation at the end of history, high pressure, distance from existing water-invaded areas, and a safe offset from other producers to minimise interference. Each candidate was tested individually using the baseline do-nothing scenario (11 producers and 5 injectors) plus one additional well. Forecasts ran from the end of history (November 2006) to January 2020. In the well control, several constraints were

applied for Scenario B in the simulation: the requested oil rate was set to 5,000 Sm3/day, the upper target liquid rate to 8,000 Sm3/day, and the minimum bottom-hole pressure to 60 bar. Cutoff limits were a maximum water cut 90 % and a maximum GOR of 1,000 Sm3/Sm3. The field injection capacity was constrained to a maximum of 42,000 Sm3/day. After evaluating the runs, the best five producers locations (P2,P10,P15,P19 and P21) were selected (see table 5 below).

Case Name	Cumulative Oil Production 10^6 sm3	Additional Oil Cumulative 10^6 Sm3
Scenario A	73.3	
Scenario A +P15	74.1	0.8
Scenario A + P10	74.0	0.7
Scenario A +P2	73.7	0.4
Scenario A +P19	73.6	0.3
Scenario A +P21	73.6	0.3

Table 5: Cumulative oil production and cumulative additional oil scenario B

A further sensitivity study was carried out to determine the optimal number of wells and their locations; results and the preferred cases are summarized in the table below, and we picked option 4 as the best case, which is the combination of producers wells (P19, P15, P10) see Table 6.

Case Name	Cumulative Oil Production 10^6 Sm3	Additional Oil Cumulative 10^6 Sm3	Cumulative water Production 10^6 Sm3
Scenario A	73.3		
Option 1 (Scenario A +P19+P10+P2)	74.1	0.8	50.1
Option 2 (Scenario A +P15+P10+P2)	74.4	1.1	47.9
Option 3 (Scenario A +P19+P15+P2)	74.3	1.0	51.1
Option 4 (Scenario A +P19+P15+P10)	74.7	1.4	50.5

Table 6: Cumulative oil production, cumulative additional oil, and cumulative water production

Figure 21 shows reservoir pressure during history and the subsequent forecast. The initial reservoir pressure was approximately 272 bar; following production, it declined rapidly, but injection-maintained reservoir pressure throughout the forecast period.

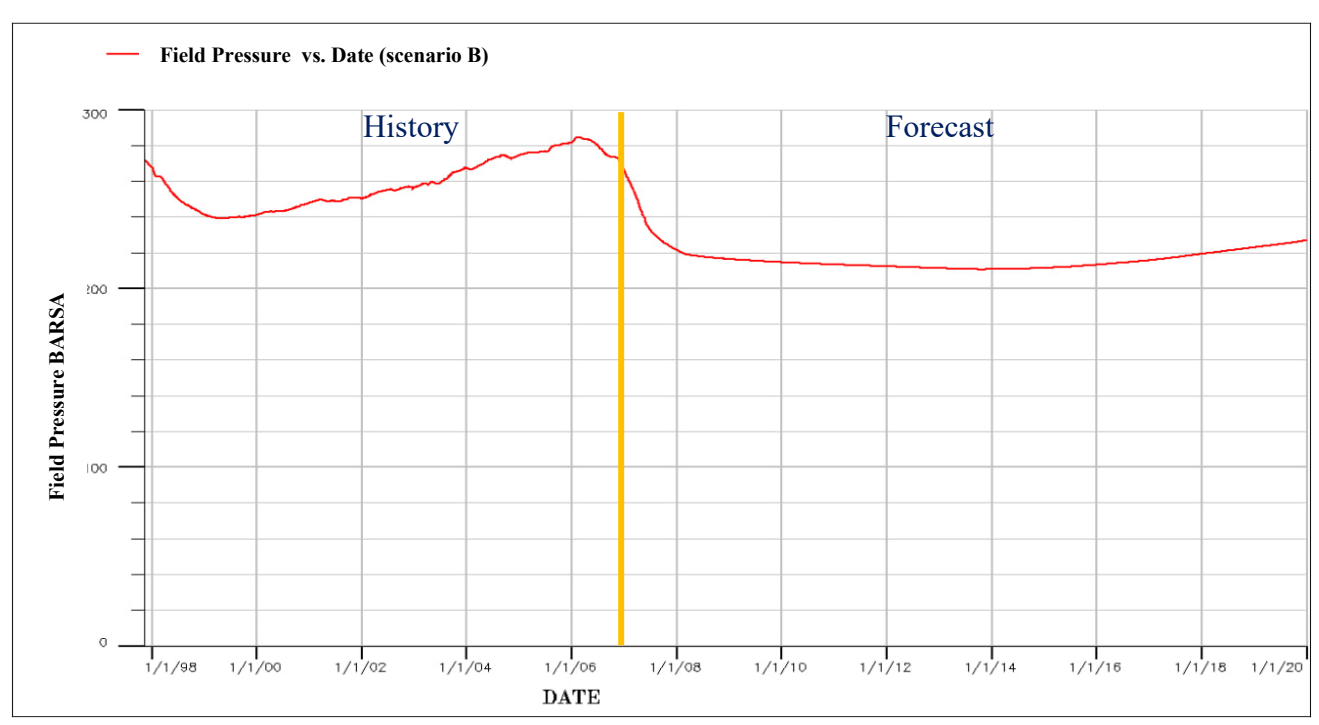


Figure 21:Field Pressure vs Time (scenario B)

Figure 22 shows the field oil production rate (FOPR) for the full history and the forecast. As we can see clearly that the production increased in 2007 due to the new production wells and reached 14000 sm3/d. Figure 23 shows the cumulative field oil production (FOPT); the forecast predicts a total recovery of approximately 74.7×10^6 Sm3 by January 2020. The recovery factor 46.7% with incremental of +0.9%.

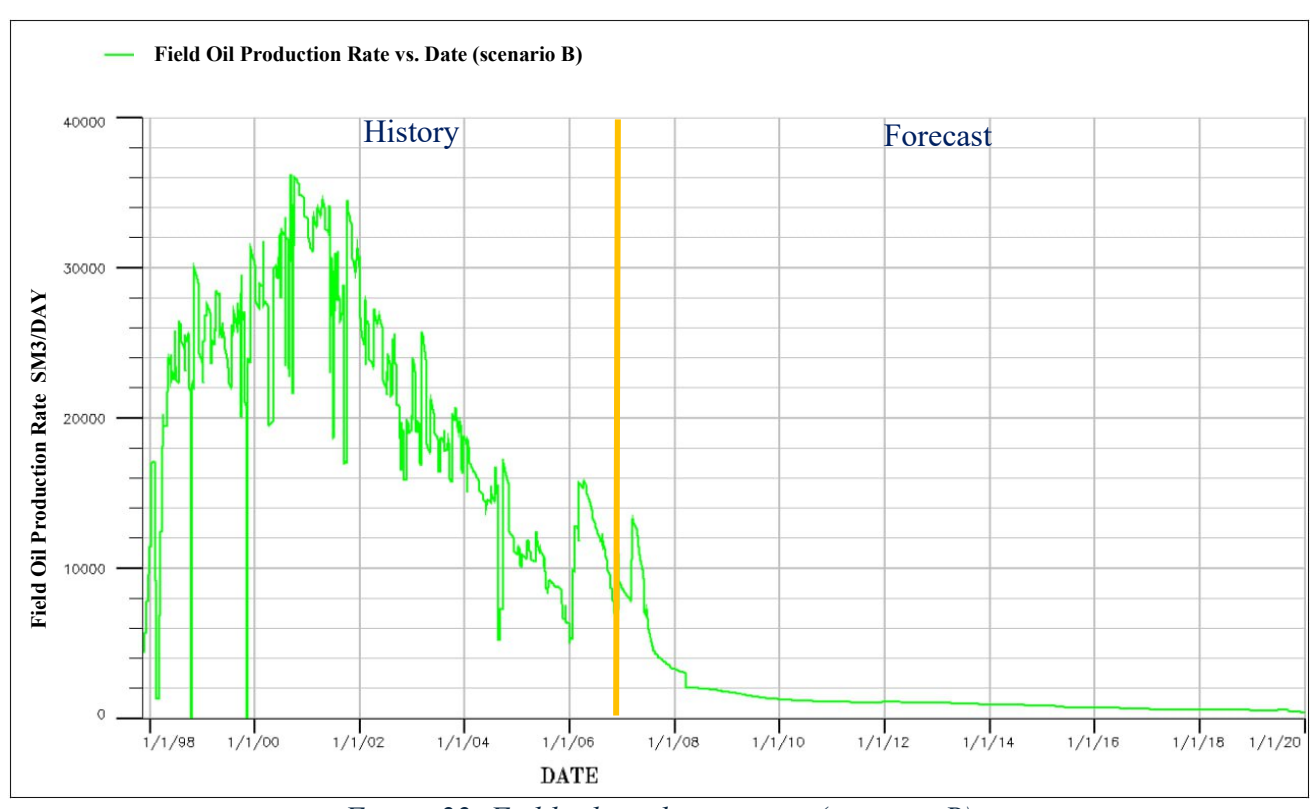


Figure 22: Field oil production rate (scenario B)

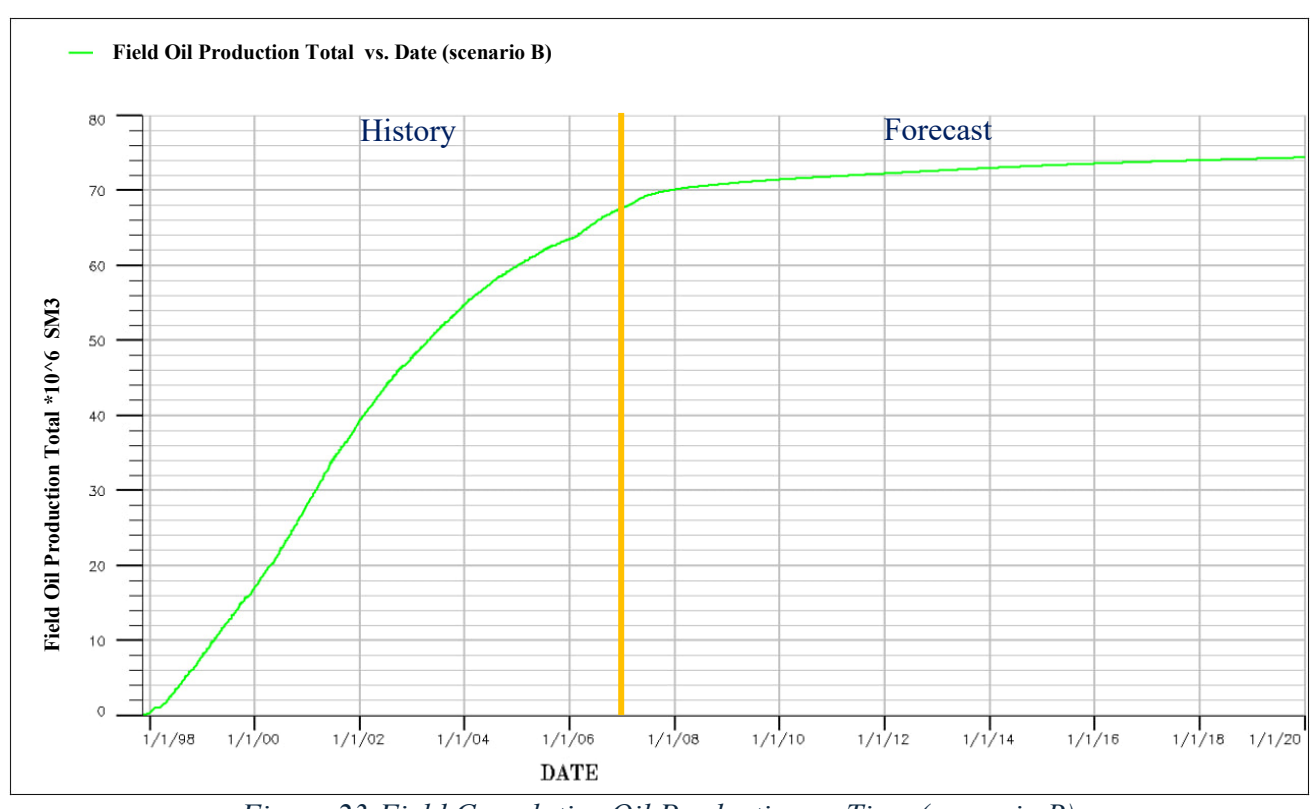


Figure 23:Field Cumulative Oil Production vs Time (scenario B)

Figure 24 shows the field gas production rate (FGPR), which follows the same to the oil rate; gas production peaked in 2001–2002 at approximately 7×10^6 Sm3/d. Figure 25 shows cumulative field gas production (FGPT); the forecast indicates it will reach approximately 18×10^9 Sm3 by January 2020. The recovery factor for gas production is 66.7%.

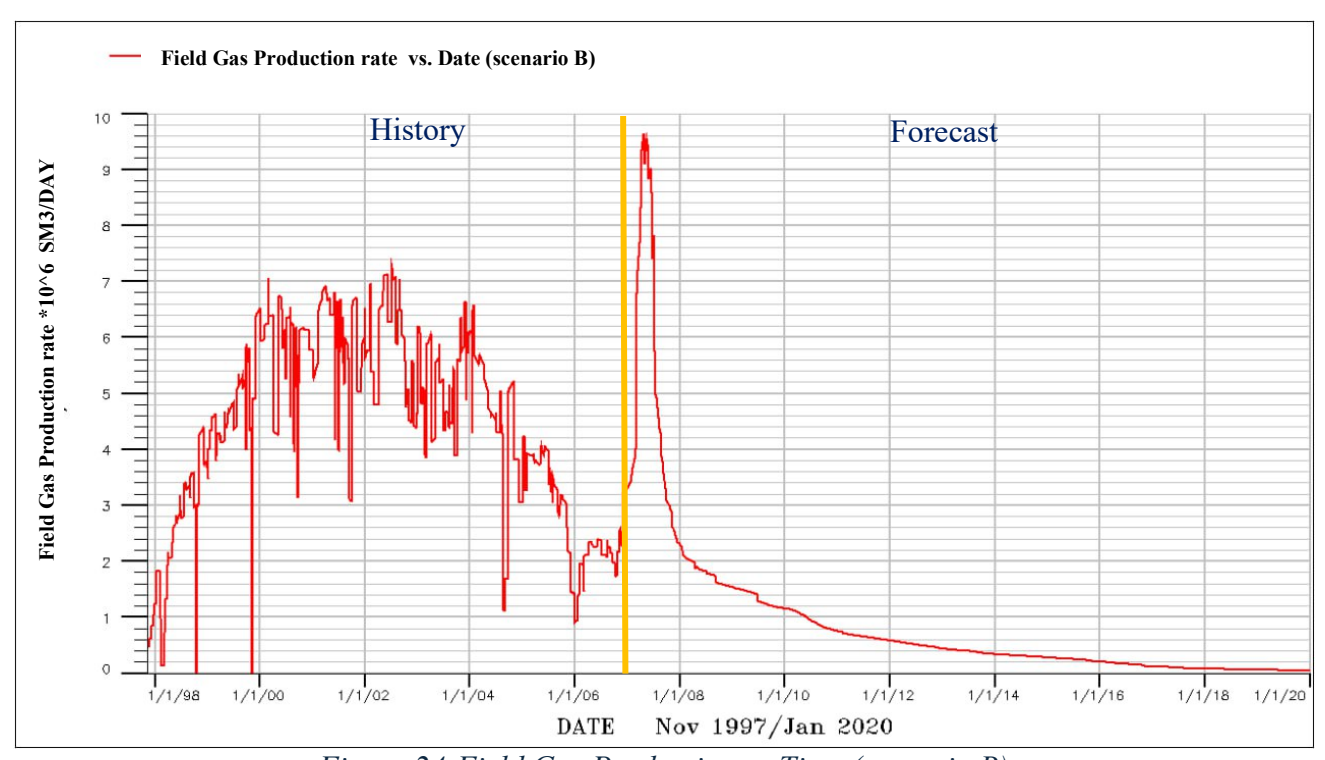


Figure 24:Field Gas Production vs Time (scenario B)

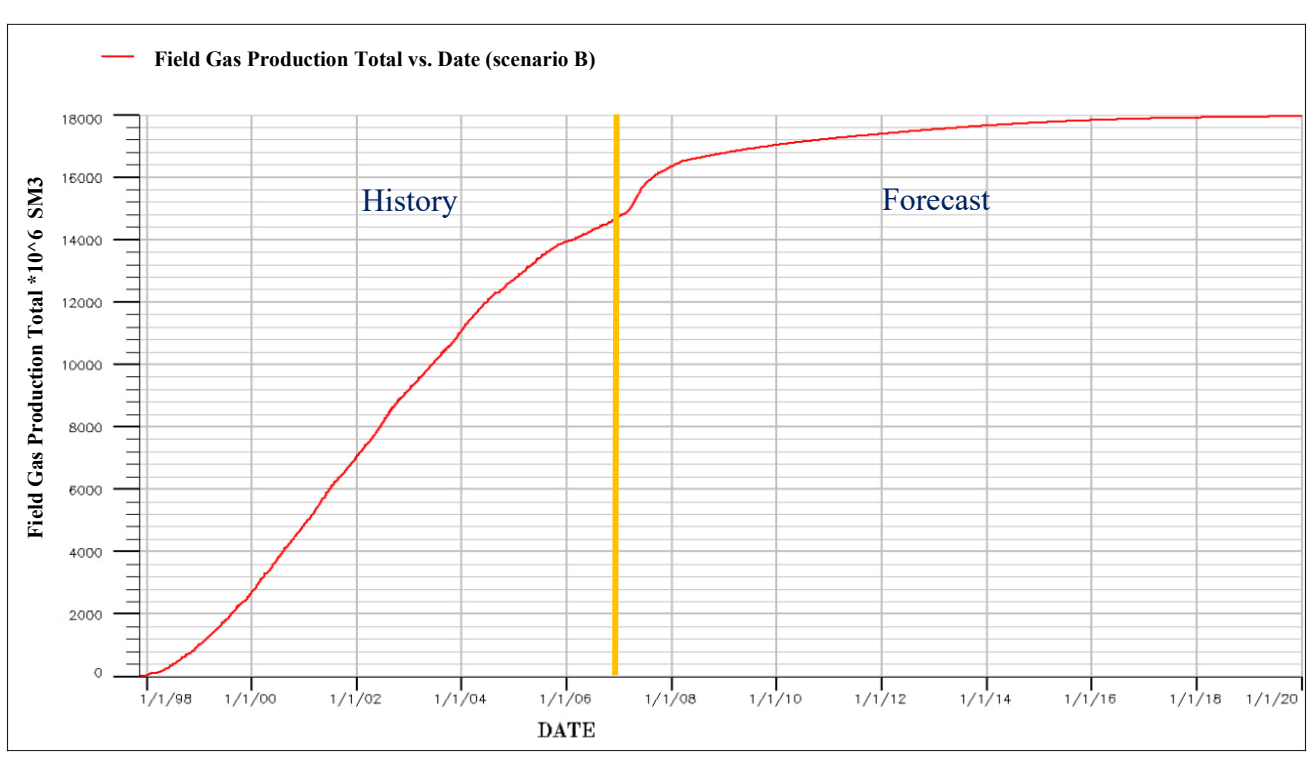


Figure 25:Field Cumulative Gas Production vs Time (scenario B)

Figure 26 shows the field water production rate (FWPR). Water breakthrough occurred in 1998, and water production steadily increased thereafter, reaching about 19,000 Sm3/day. The rising water cut negatively impacts oil production, so mechanical water-shutoff interventions were executed to preserve oil rates. Figure 27 shows cumulative field water production (FWPT), which reaches approximately 50.5 × 10⁶ Sm3 by the end of field life in January 2020. Figure 28 shows field water injection rates; injection increased over the field life to a maximum of about 50,000 Sm3/d, and at the beginning of 2006, injection was reduced as the pressure decline eased following the drop in oil production.

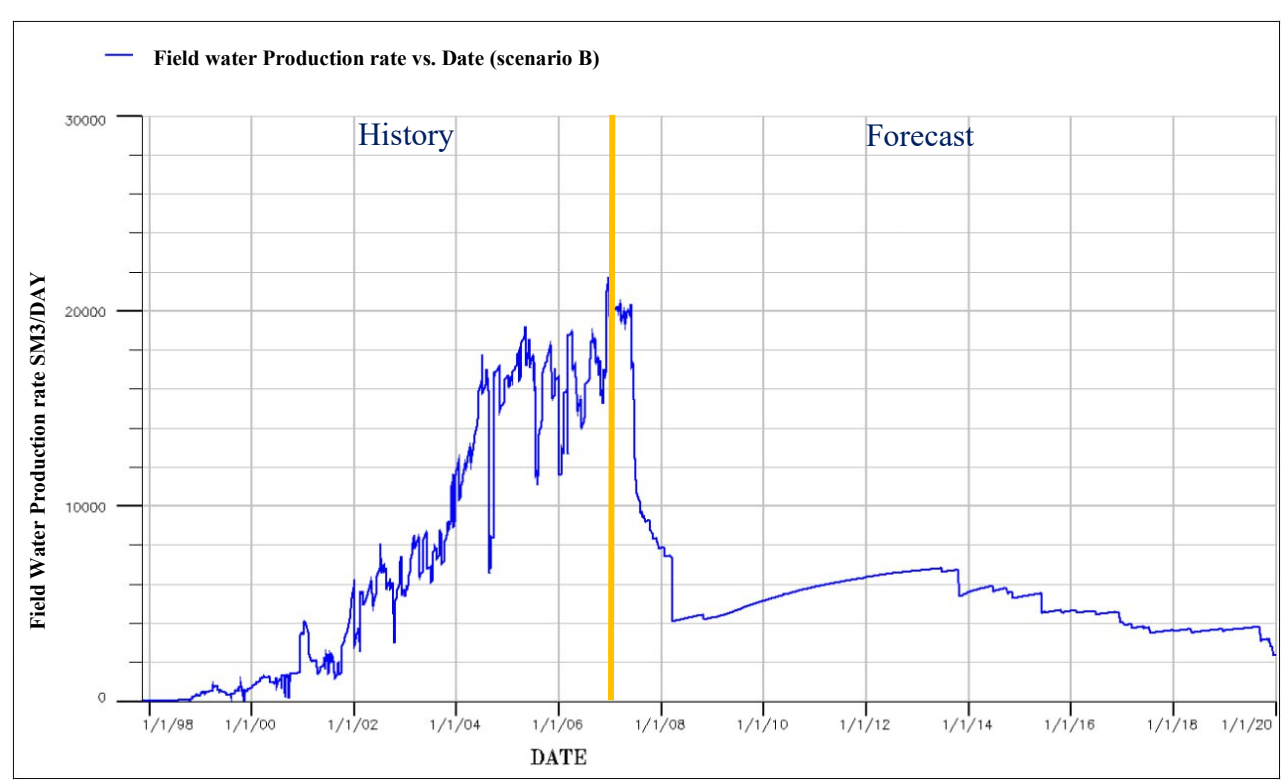


Figure 26: Field water production rate vs Time (scenario B)

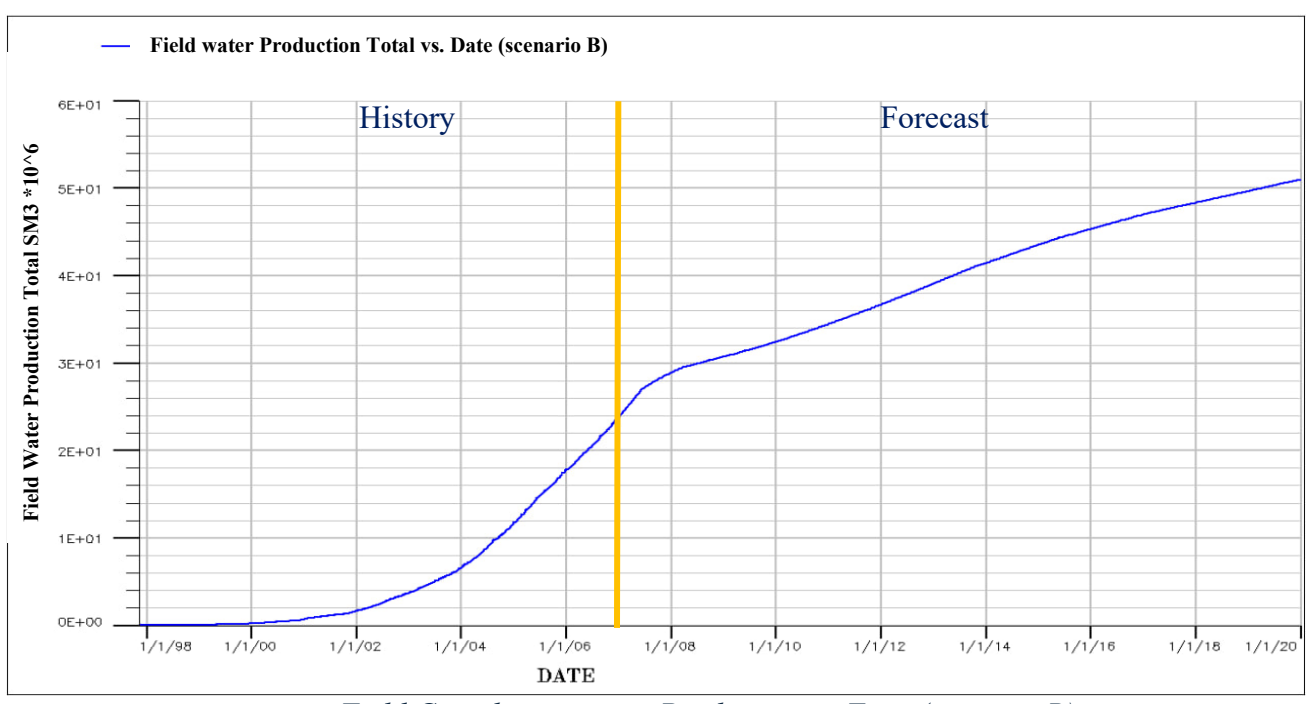


Figure 27: Field Cumulative water Production vs Time (scenario B)

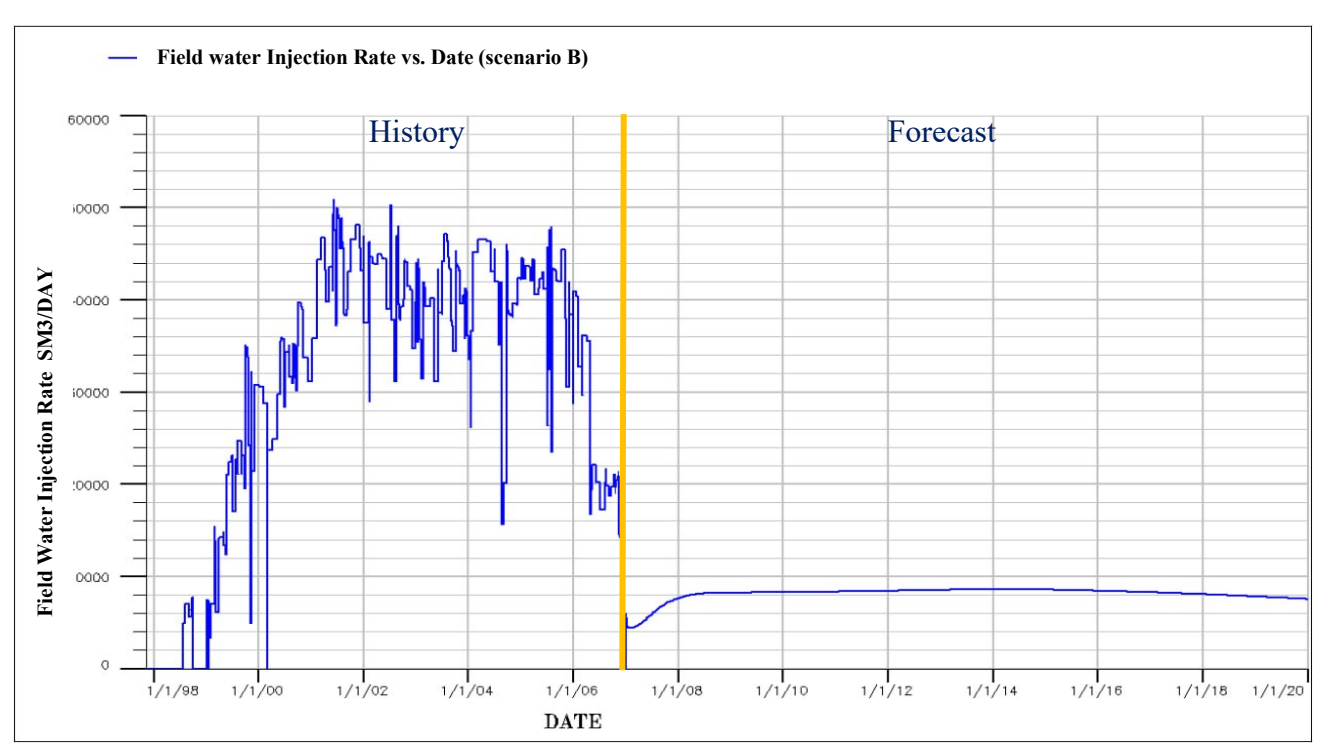


Figure 28: Field water injection rate (scenario B)

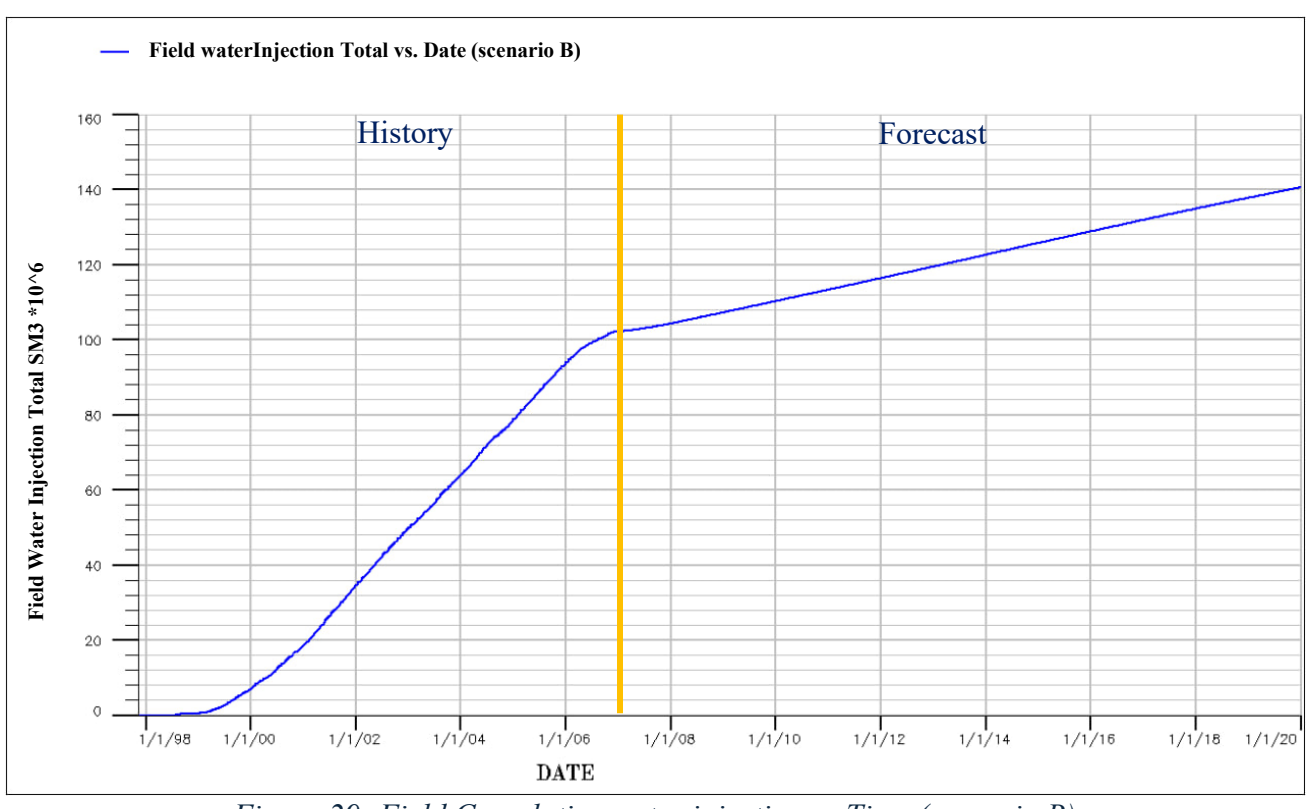


Figure 29: Field Cumulative water injection vs Time (scenario B)

At the end of history (Nov 2006), the proposed P-19 location lies within a remaining oil accumulation (localized high-oil-saturation zone), indicating a strong infill opportunity. By Jan 2020 (post-P-19), the same area is visibly depleted, reflecting effective drainage and good interwell connectivity. The Figures 30 at the end of history & Figure 31 at the end of forecast show the two saturation maps to illustrate the depletion of the remaining oil accumulation.

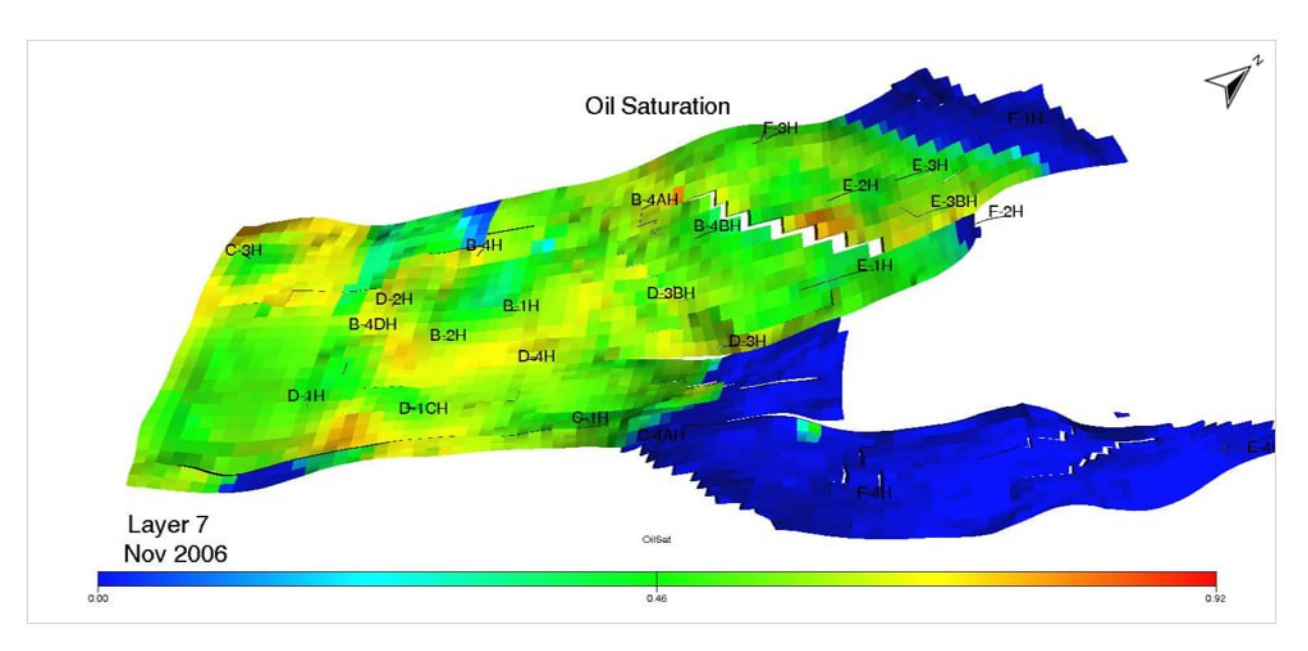


Figure 30: Layer 7 Oil Saturation (Nov 2006): P-19 target area and remaining-oil accumulation.

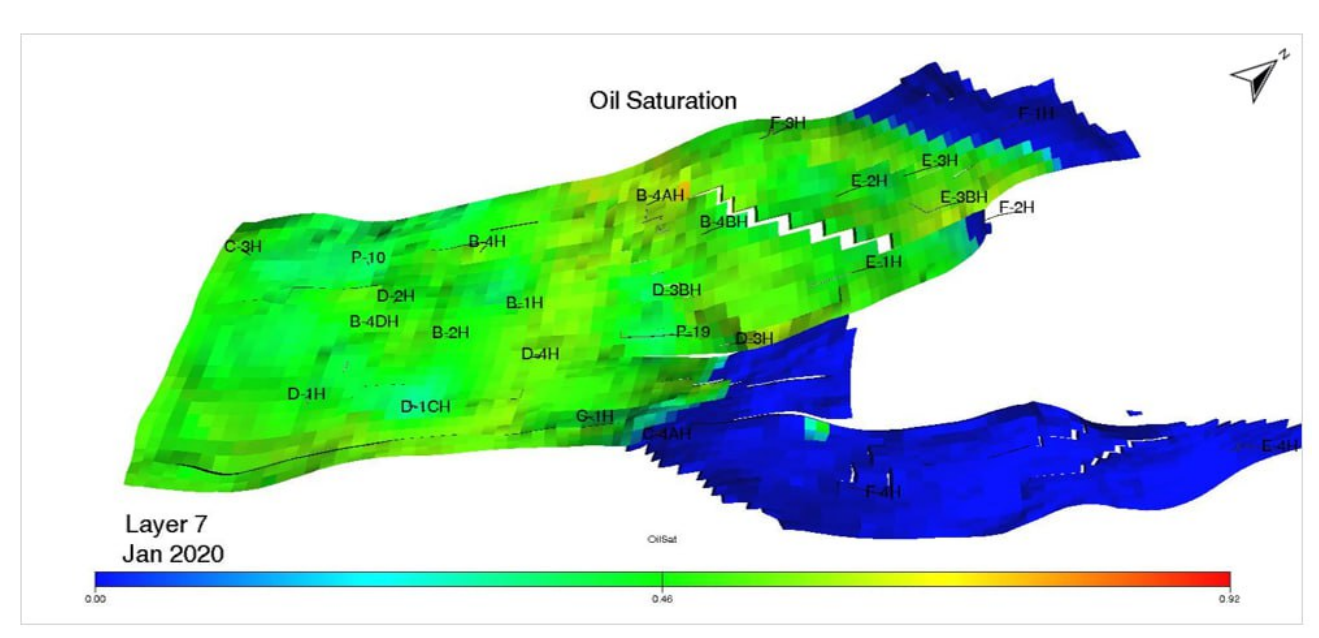


Figure 31:Layer 7 Oil Saturation (Jan 2020): Depletion of the P-19 remaining-oil accumulation.

At the end of history (Nov 2006), the proposed P-10 location lies within a remaining oil accumulation (localized high-oil-saturation zone), indicating a strong infill opportunity. By Jan 2020 (post-P-10), the same area is visibly depleted, reflecting effective drainage and good interwell connectivity. The Figures 32 at the end of history & Figure 33 at the end of forecast show the two saturation maps to illustrate the depletion of the remaining oil accumulation.

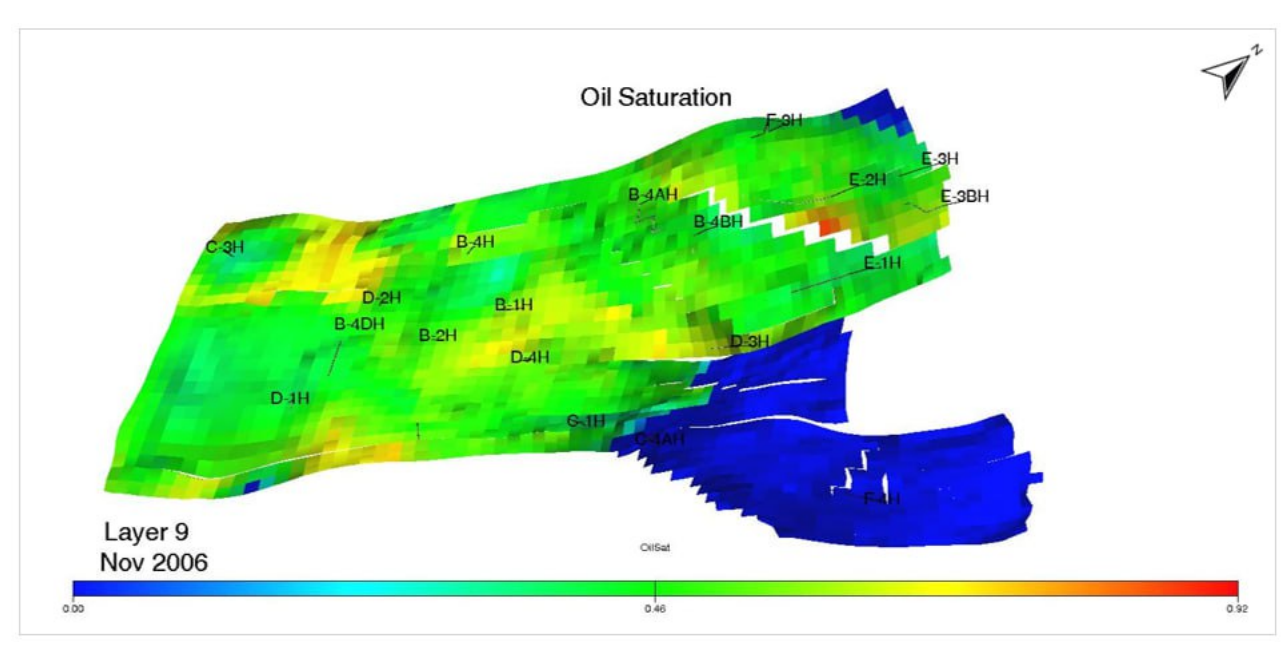


Figure 32: Layer 9 Oil Saturation (Nov 2006): P-10 target area and remaining-oil accumulation

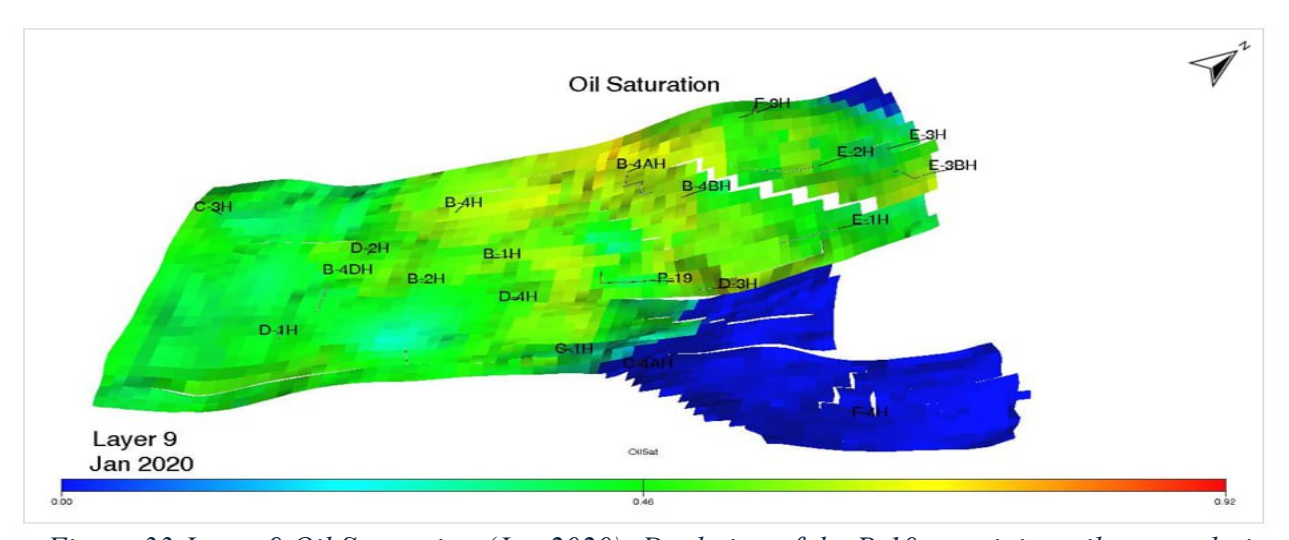


Figure 33:Layer 9 Oil Saturation (Jan 2020): Depletion of the P-10 remaining-oil accumulation

At the end of history (Nov 2006), the proposed P-15 location lies within a remaining-oil accumulation (localized high-oil-saturation zone), indicating a strong infill opportunity. By Jan 2020 (post-P-15), the same area is visibly depleted, reflecting effective drainage and good interwell connectivity. The Figures 34 at the end of history & Figure 35 at the end of forecast show the two saturation maps to illustrate the depletion of the remaining oil accumulation.

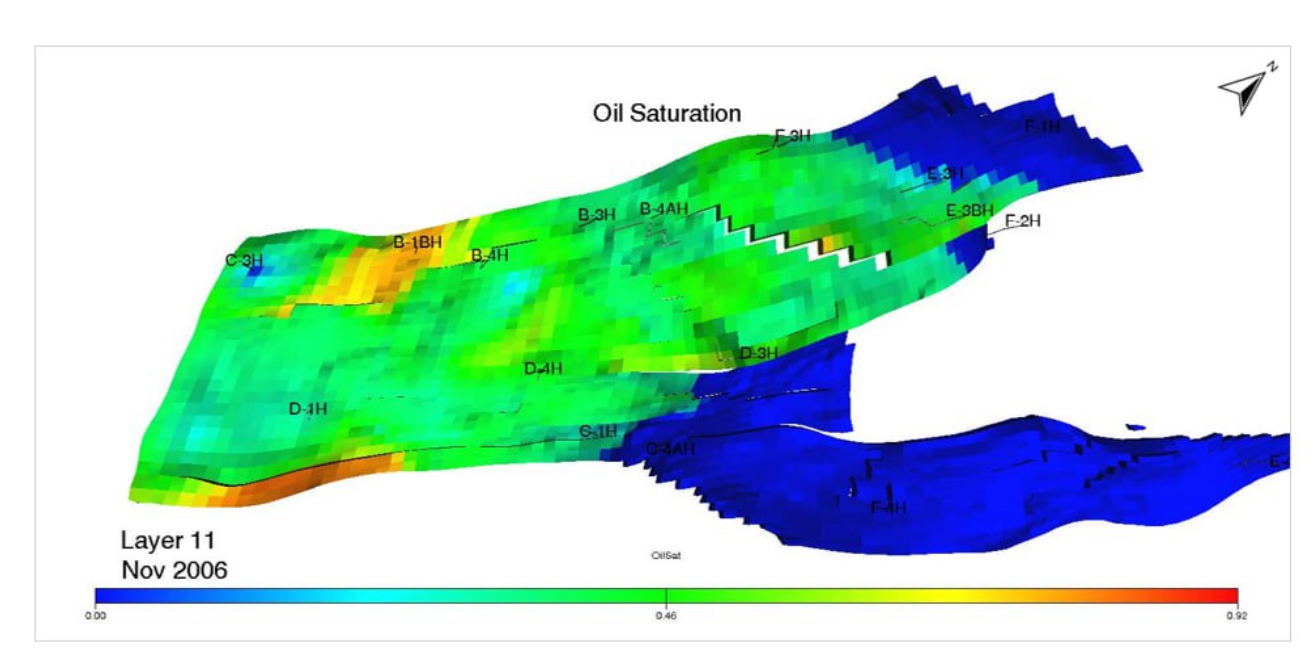


Figure 34:Layer 11 Oil Saturation (P-15 Target Area): Nov 2006 vs Jan 2020

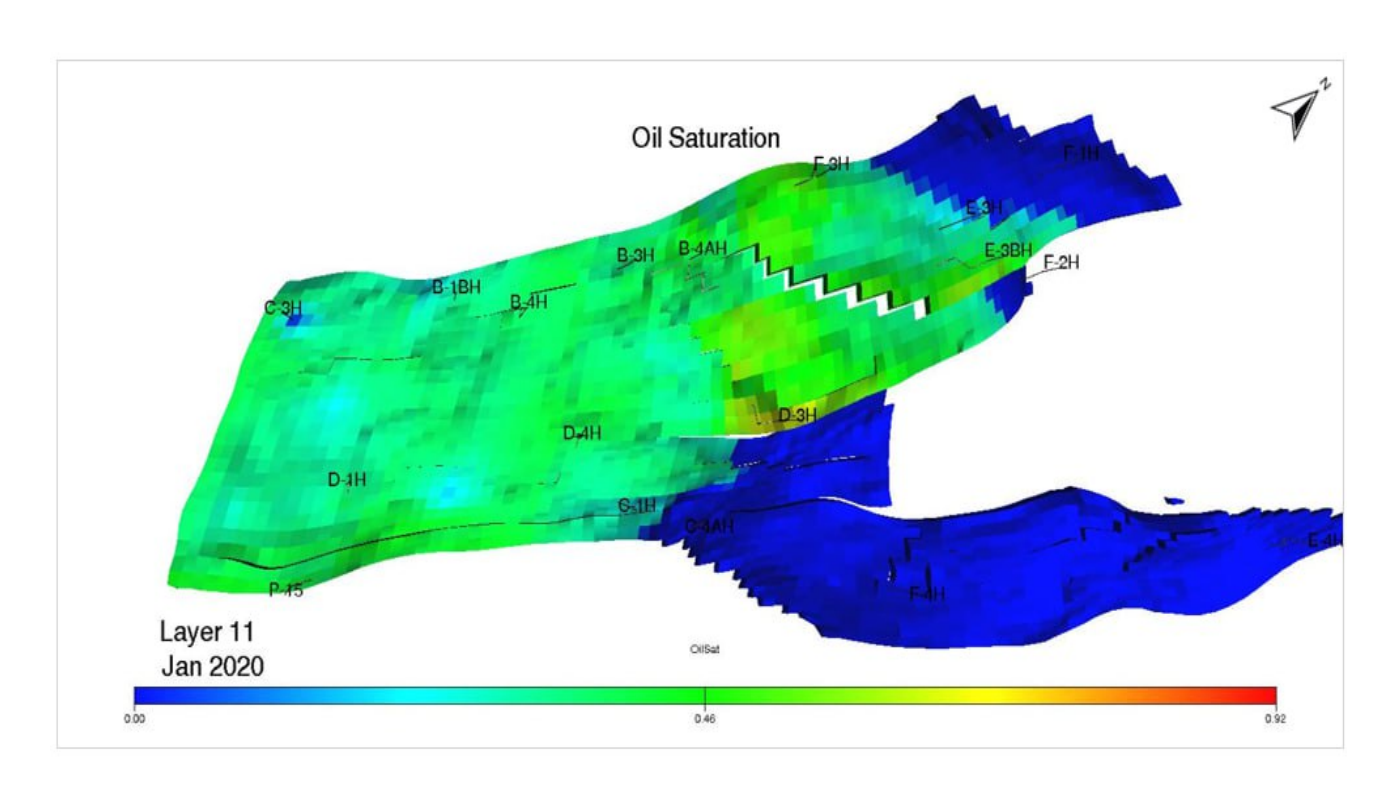


Figure 35: Layer 11 Oil Saturation (Jan 2020): Depletion of the P-15 remaining-oil accumulation

Figures 30–35 demonstrate that the high-oil-saturation regions present at end of history (Nov 2006) are substantially reduced by January 2020, following the drilling of new producers—optimally P-15, P-19, and P-21. The observed reduction indicates localized depletion and improved sweep, reflecting effective drainage and robust interwell connectivity.

4.3 Scenario C: Scenario B(option 4) + new injection wells

In this scenario, an IOR strategy was implemented to improve oil recovery by adding new injection wells. The dynamic model was used to forecast reservoir performance with the additional injectors. A sensitivity study was performed on Scenario B (existing wells plus three new producers): injectors were added one at a time at candidate locations, and each run was evaluated for incremental oil recovery. After testing multiple locations, seven injectors (I1,I2,I3,I4,I5,I6,I7) were selected (see Table 7 below).

Location selection criteria included: low-pressure zones at the end of history, remaining oil in place, favourable petrophysical properties, and positions that would promote effective sweep toward existing producers.

Case Name	Cumulative Oil Production 10^6 Sm3	Additional Oil Cumulative 10^6 Sm3
Scenario B	74.7	
Scenario B+I1	76.0	1.4
Scenario B+I2	75.5	0.9
Scenario B+I3	76.1	1.4
Scenario B+I4	75.8	1.2
Scenario B+I5	75.7	1.1
Scenario B+I6	75.8	1.1
Scenario B+I7	75.8	1.2

Table 7: Cumulative oil production and cumulative additional oil scenario C

A final sensitivity study was conducted to optimize both the number and placement of the selected injectors; the preferred injector configurations are summarized in Table 8 below. According to the results, we chose option 1 as the best case, and regarding option 4, we excluded it due to high cumulative water production. The injector wells are shown in the Figure 36.

Case Name	Cumulative Oil Production 10^6 Sm3	Additional Oil Cumulative 10^6 Sm3	Cumulative water Production 10^6 Sm3
Scenario B	74.7		
Option 1 (Scenario B+ I2+I3+I4)	77.2	2.5	68.8
Option 2 (Scenario B+ I1+I3+I7)	76.9	2.3	69.4
Option 3 (Scenario B+ I1+I4+I5)	76.6	1.9	68.1
Option 4 (Scenario B+ I5+I6+I7)	77.3	2.7	74.1

Table 8: Cumulative oil production, cumulative additional oil, and cumulative water production scenario C

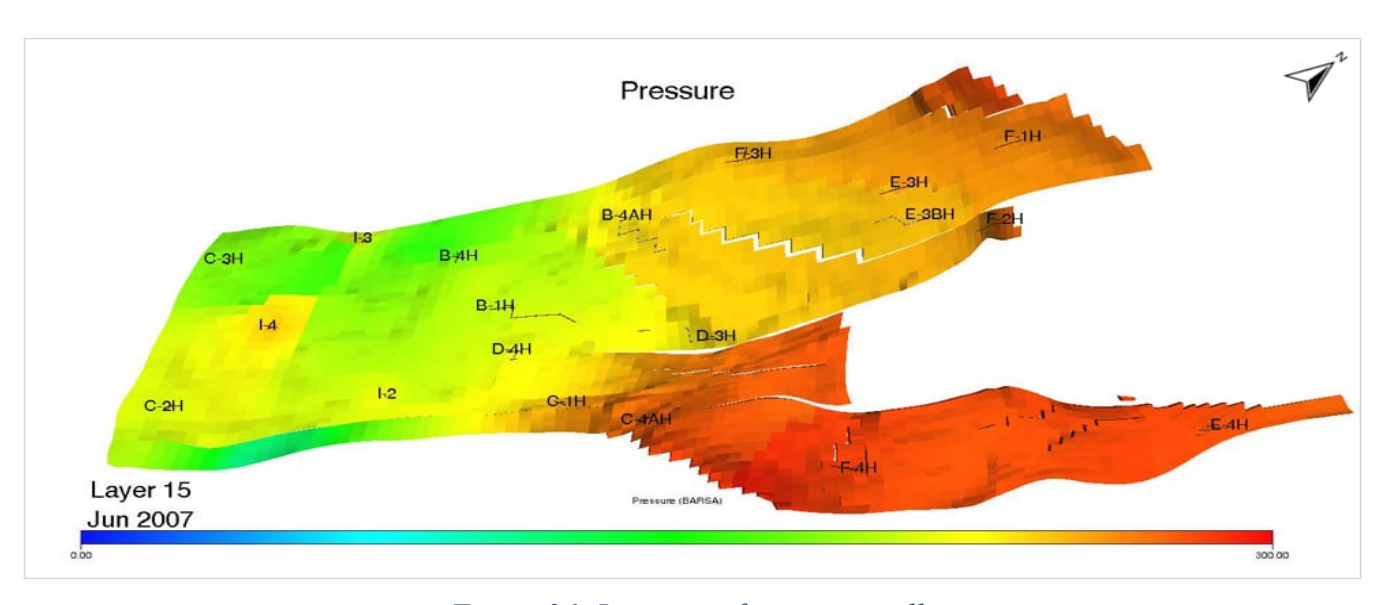


Figure 36: Location of injection wells

Figure 37 shows reservoir pressure during history and the subsequent forecast. The pressure shows an increase around 60 bar from 2007 to 2020 due to the injection of new injection wells (I2, I3, I4)

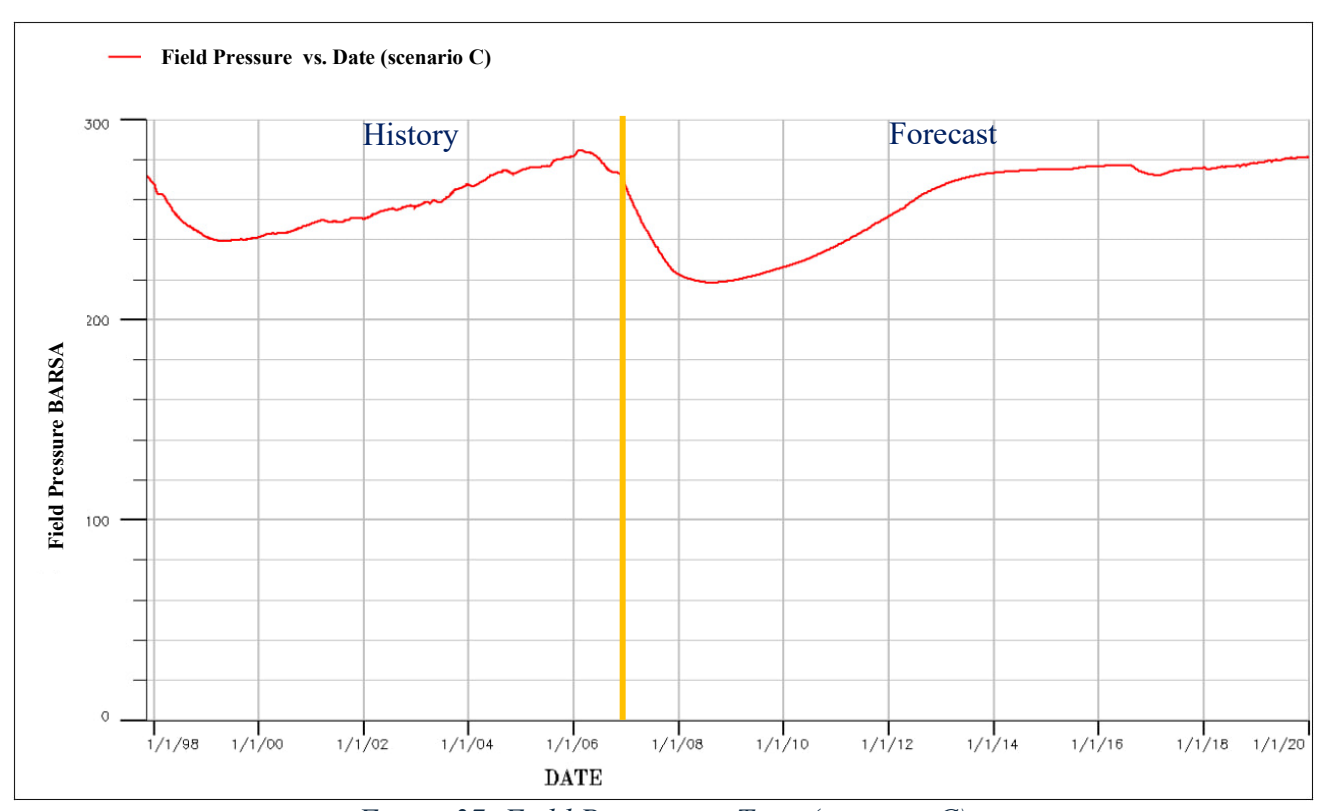


Figure 37: Field Pressure vs Time (scenario C)

Figure 38 shows the field oil production rate (FOPR) for the full history and the forecast. As we can see clearly that the production increased in 2007 due to the new injection wells and reached 14000 sm3/d. Figure 39 shows the cumulative field oil production (FOPT); the forecast predicts a total recovery of approximately 77.2×10^6 Sm3 by January 2020. The recovery factor for oil production is 48.3 % and the incremental recovery factor compared Scenario A (Do Nothing) is 2.4 %.

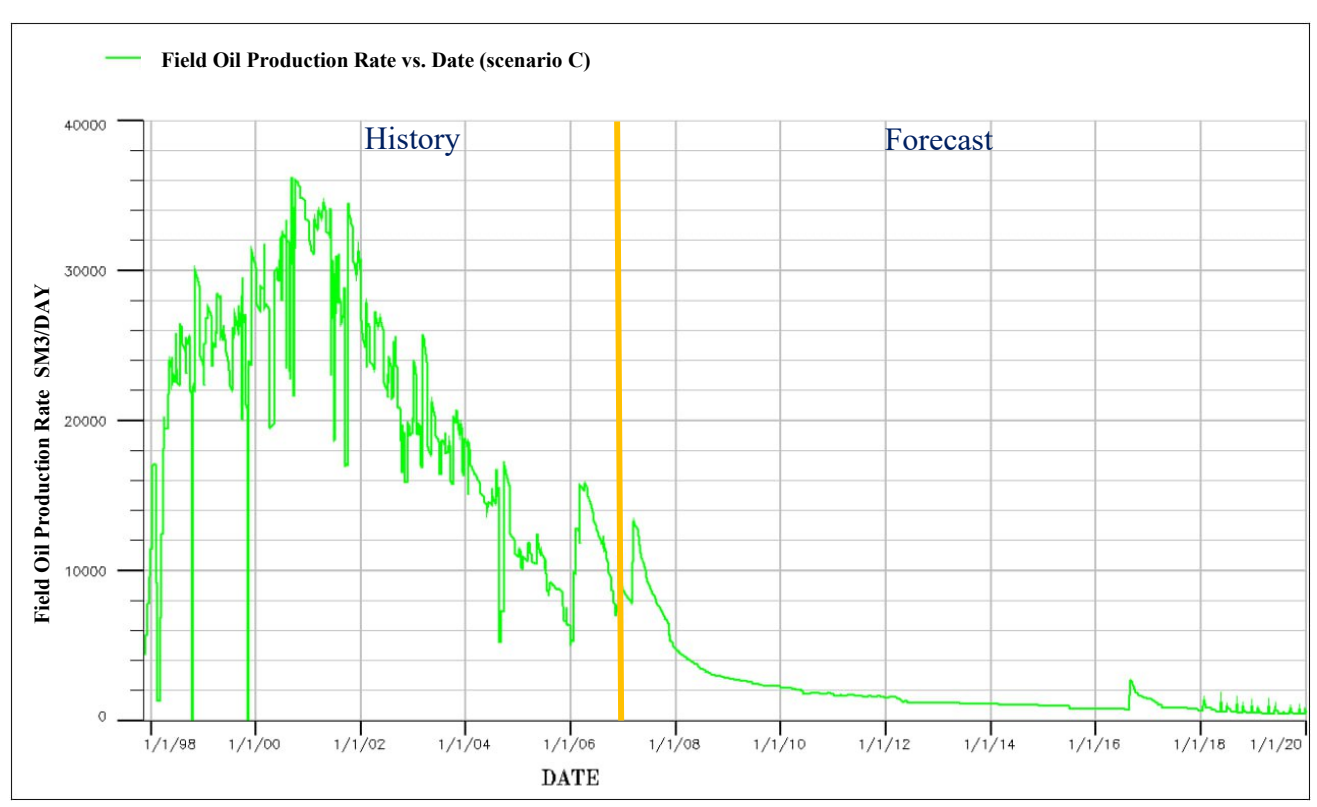


Figure 38: Field oil production rate (scenario C)

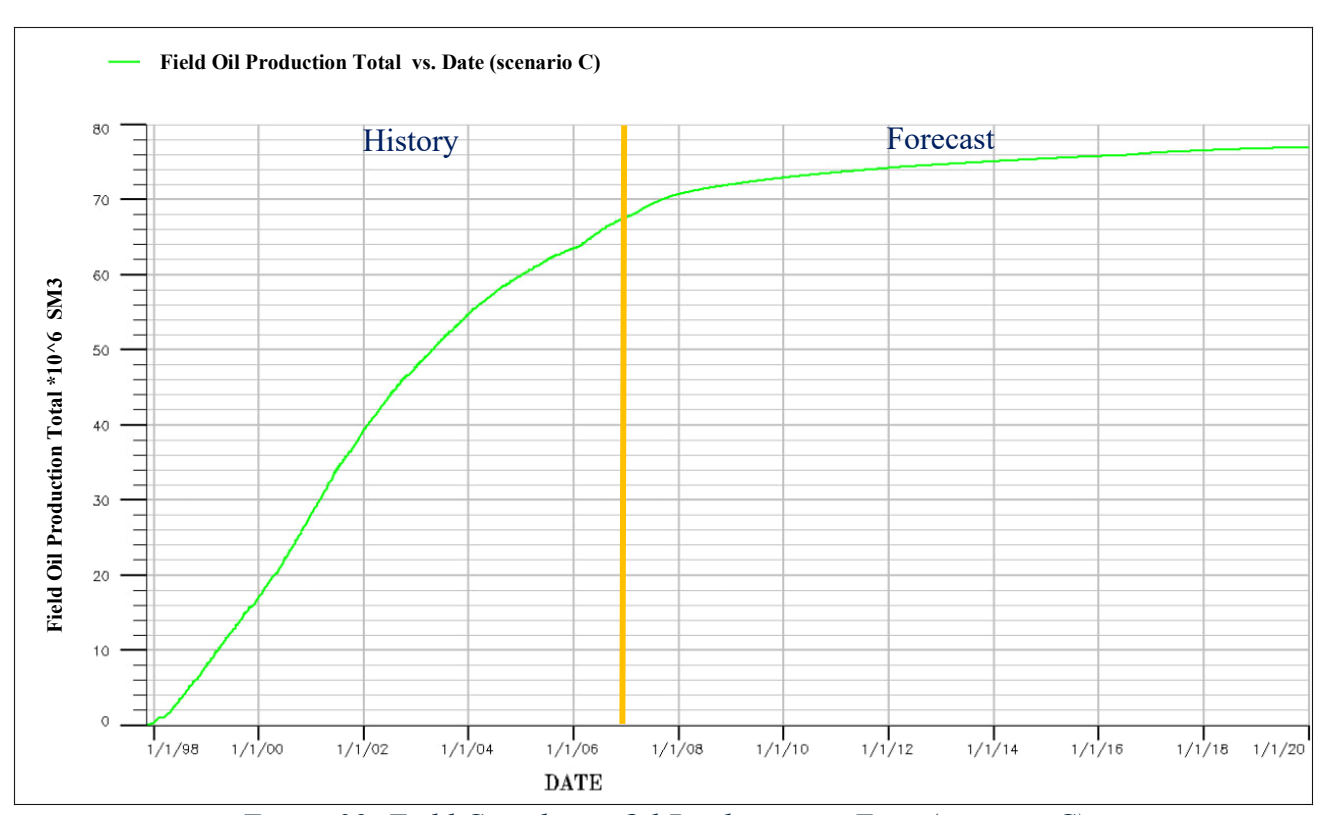


Figure 39: Field Cumulative Oil Production vs Time (scenario C)

Figure 40 shows the field gas production rate (FGPR), which follows the same to the oil rate; gas production peaked in 2001–2002 at approximately 7×10^6 Sm3/d. Figure 41 shows cumulative field gas production (FGPT); the forecast indicates it will reach approximately 18×10^9 Sm3 by January 2020. The recovery factor for gas production is 66.7%.

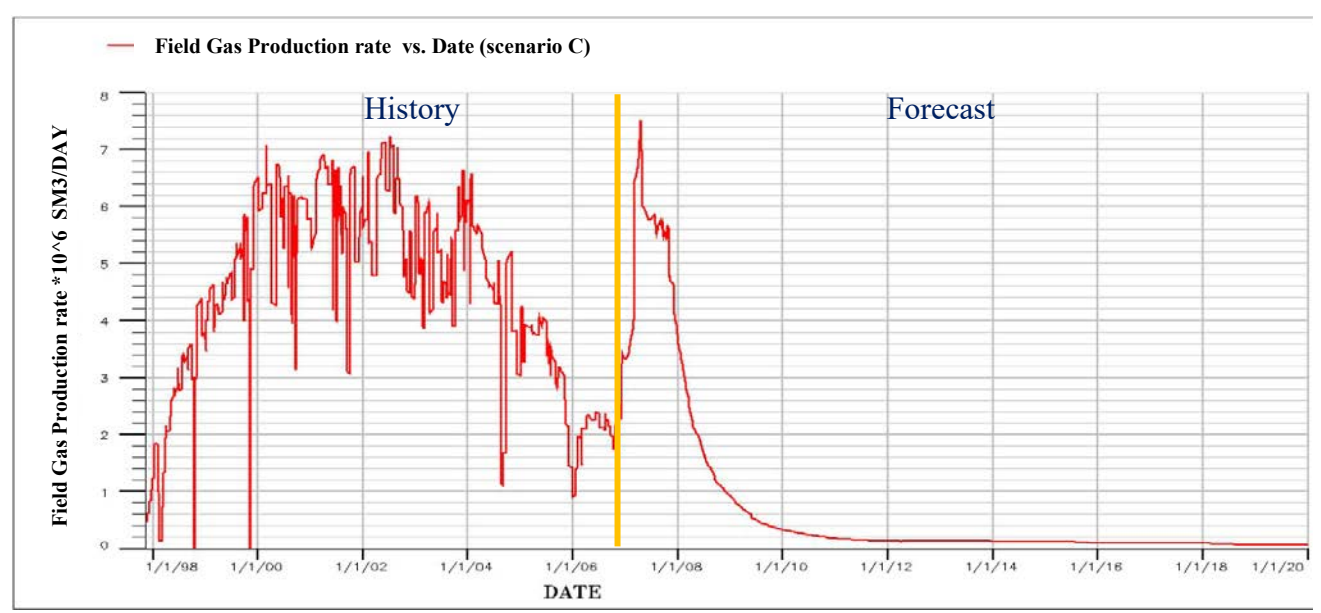


Figure 40: Field Gas Production vs Time (scenario C)

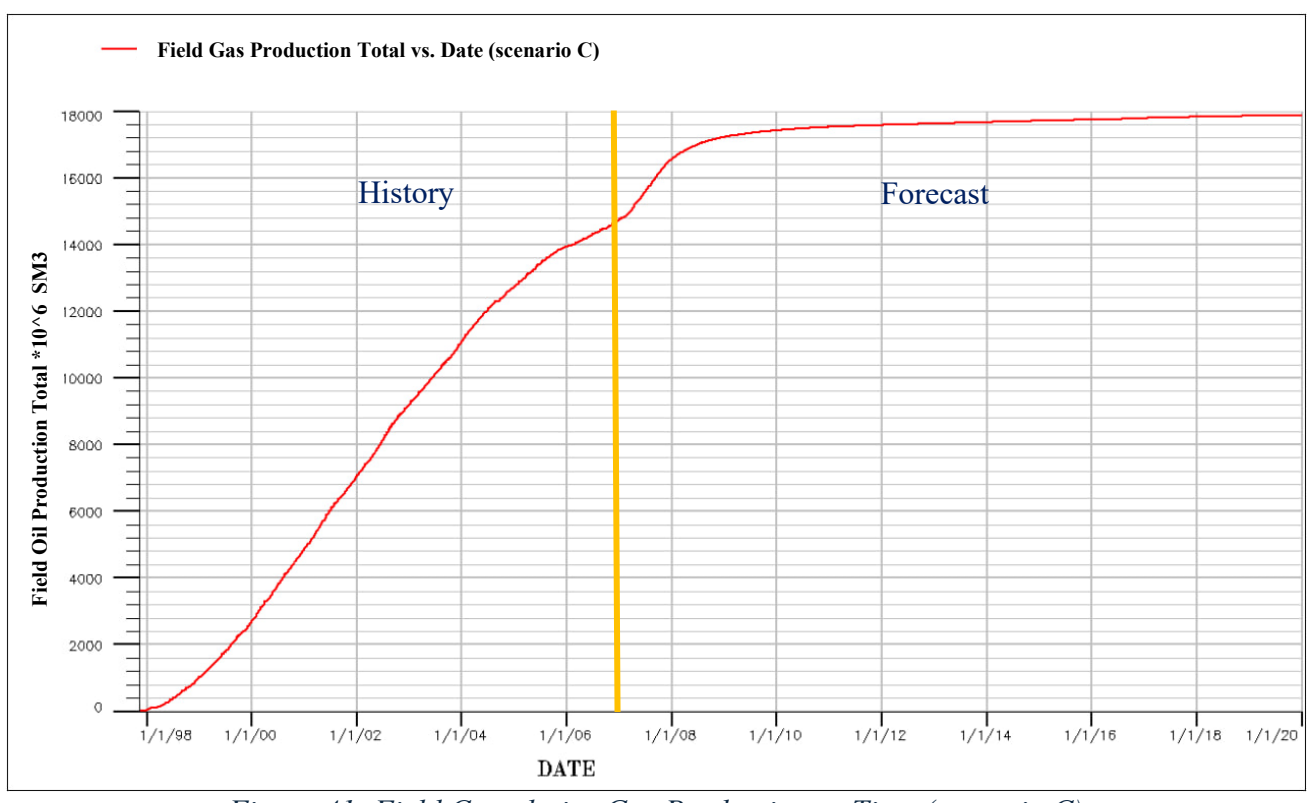


Figure 41: Field Cumulative Gas Production vs Time (scenario C)

Figure 42 shows the field water production rate (FWPR). Water breakthrough occurred in 1998, and water production steadily increased thereafter, reaching about 19,000 Sm3/day. The rising water cut negatively impacts oil production, so mechanical water-shutoff interventions were executed to preserve oil rates. Figure 43 shows cumulative field water production (FWPT), which reaches approximately 69.5 × 10⁶ Sm3 by the end of field life in January 2020. Figure 44 shows field water injection rates; injection increased over the field life to a maximum of about 50,000 Sm3/d, and at the beginning of 2006, injection was reduced as the pressure decline eased following the drop in oil production.

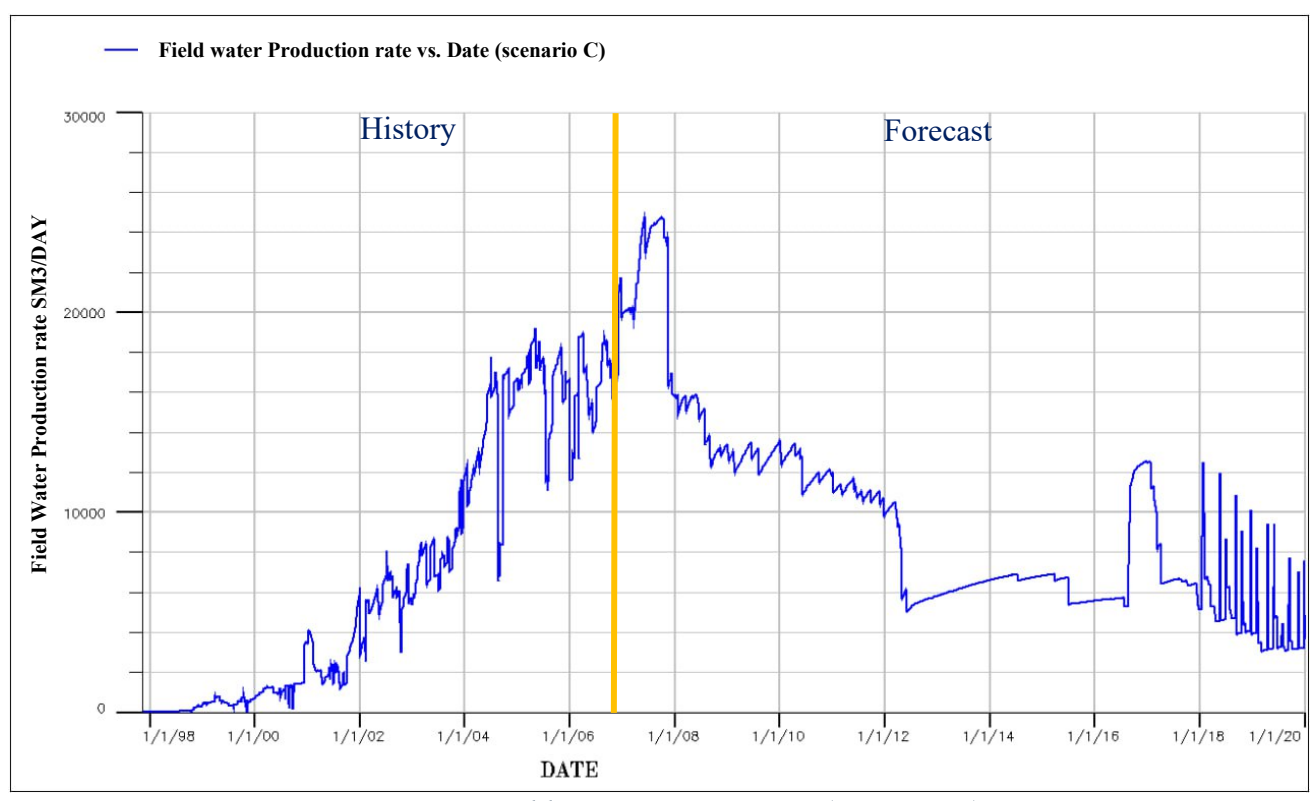


Figure 42: Field water injection rate (scenario C)

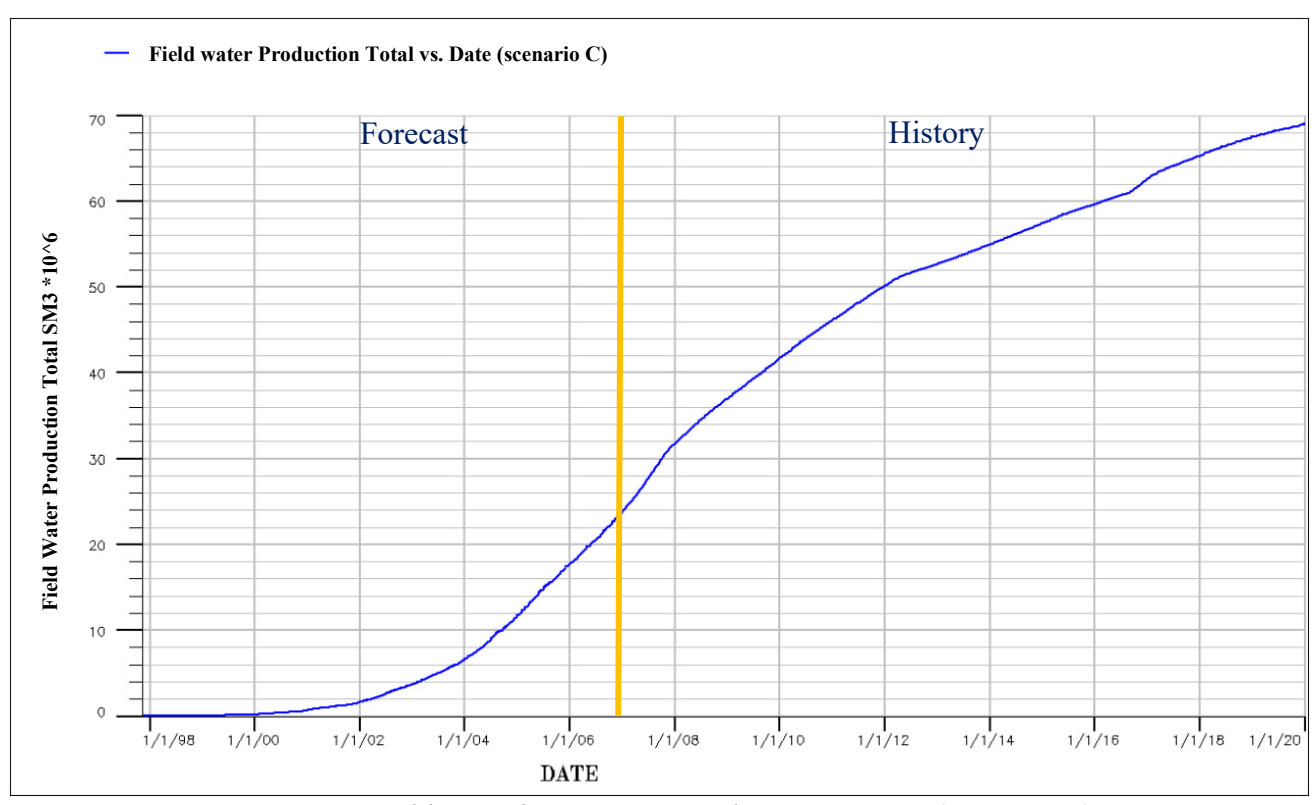


Figure 43:Field Cumulative water production vs Time (scenario C)

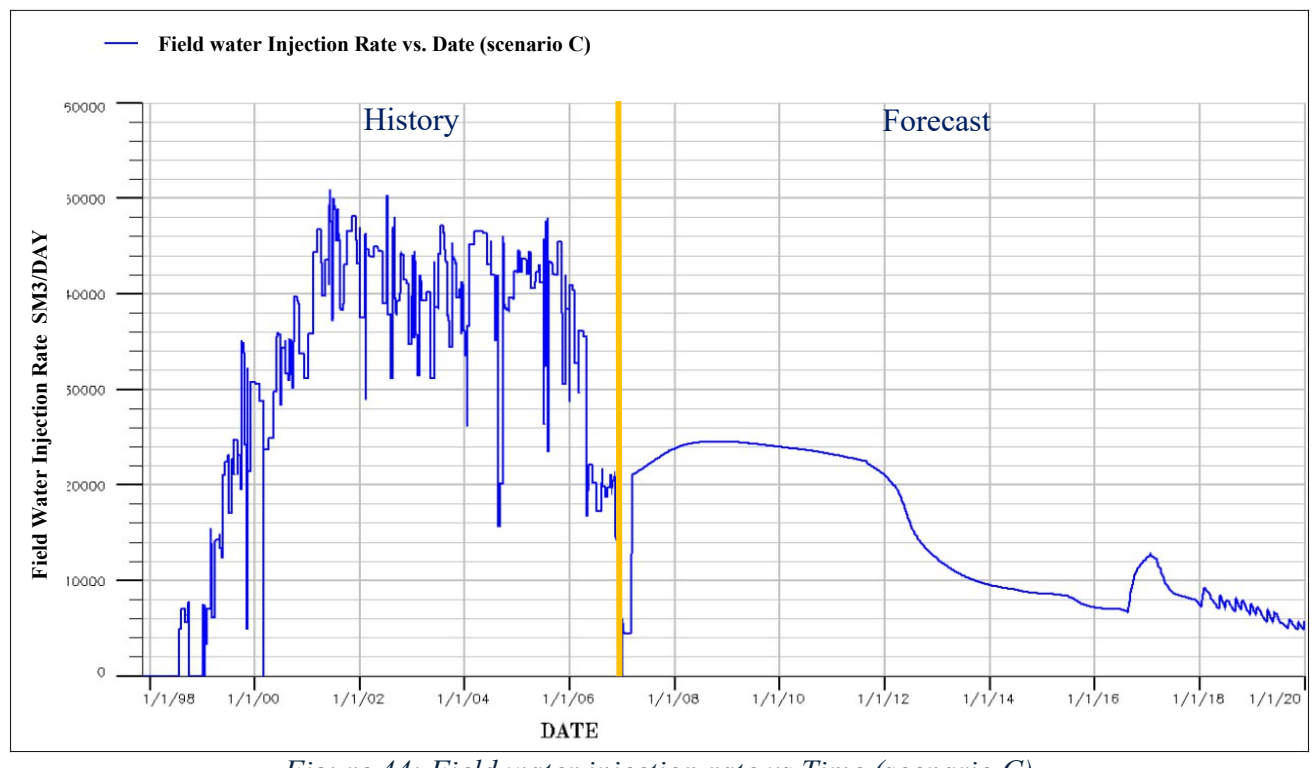


Figure 44: Field water injection rate vs Time (scenario C)

Table 9 summarizes the recovery factor (RF) and cumulative production for the three scenarios. Scenario A attains an RF of 45.8%. Relative to Scenario A, Scenario B increases RF by 0.9 percentage points to 46.7%, while Scenario C provides the largest gain, rising by 2.4 % to 48.3%. The table also reports cumulative oil, water, and gas to January 2020 for each case, showing that Scenario C achieves the highest cumulative oil $(77.2 \times 10^{6} \text{ Sm}^{3})$ but with a substantial increase in cumulative water (69.5 $\times 10^{6} \text{ Sm}^{3}$), whereas cumulative gas remains essentially unchanged ($\approx 18 \times 10^{9} \text{ Sm}^{3}$).

	Scenario A	Scenario B	Scenario C
Recovery factor (RF) %	45.8	46.7	48.3
Cumulative oil production Sm3	73.3 × 10^6	74.7 × 10^6	77.2 × 10^6
Cumulative water production Sm3	49.2 × 10^6	50.5 × 10^6	69.5 × 10^6
Cumulative gas production Sm3	17.6 × 10^9	18× 10^9	18× 10^9

Table 9: Final results for all scenarios

5. Conclusion and Future Work

This study evaluated Improved Oil Recovery (IOR) option for the mature, compartmentalized Norne Field using a 3D numerical model. Starting from a history-consistent state at end-2006, three forward scenarios were assessed under realistic operating and facility constraints to determine how water injection and well placement can extend field life and increase recovery.

The Do-Nothing basecase captures only the declining tail of the legacy waterflood, providing a benchmark trajectory for pressure, rates, and cumulative recovery. Forecast results indicate that, with existing wells and controls, cumulative oil would reach ~73.3×10⁶ Sm³ by January 2020, confirming limited remaining potential without targeted interventions.

Adding selected new producers (Scenario B) increases field production, lifting cumulative oil to about 74.7×10⁶ Sm³ by 2020. The infill program's impact is strongest where local pressure support is adequate and well placement honors high oil saturation, good permeability, porosity, high-NTG targets, and interference constraints. These outcomes underscore that producer additions alone can deliver meaningful, but context-dependent, gains in compartmentalized settings.

Introducing additional injectors (Scenario C) delivered the largest and most robust uplift across the evaluation window, with cumulative oil rising to ~77.2×10⁶ Sm³. The injector program sustains higher average reservoir pressure and improves areal/vertical sweep while remaining within initial reservoir pressure, safety margins and facility water-handling limits, indicating a more defensible path to latelife value creation.

Oil saturation maps for locations such as P-19 (Layer 7), P-10 (Layer 9), and P-15 (Layer 11) sat over remaining-oil accumulations at end-history (Nov-2006) and show clear depletion by 2020, evidencing dynamic connectivity and effective drainage when developed and/or supported by nearby injectors. This validates the combined strategy of infill producers for access plus injectors for recovery improvement.

Regarding the limitations, the results depend on the accuracy of the static/dynamic models (rock properties, contacts, pressures, relative permeability, capillary functions) and on assumed operating constraints (BHP caps, cut-offs, facility capacities). Also, further calibration can be done, such as expanded history matching could reduce the uncertainties.

In summary, the most defensible IOR path for Norne-type reservoirs combines selective infill producers with a purpose-built injector program to improve oil production, implemented within a rigorous, uncertainty-aware simulation framework and tied to economic decision criteria.

6. References

Aderibigbe, A., Cheng, K., Heidari, Z., Killough, J., & Fuss-Dezelic, T. (2016). Application of magnetic nanoparticles mixed with propping agents in enhancing near-wellbore fracture detection. Journal of Petroleum Science & Engineering, 141, 133–143. https://doi.org/10.1016/j.petrol.2016.01.027

Alvarado, V., & Manrique, E. (2010). Enhanced oil recovery: An update review. Energies, 3(9), 1529–1575. https://doi.org/10.3390/en3091529

Amid, A., Mignard, D., & Wilkinson, M. (2016). Seasonal storage of hydrogen in a depleted natural gas reservoir. International Journal of Hydrogen Energy, 41(12), 5549–5558. https://doi.org/10.1016/j.ijhydene.2016.02.036

Bradley, H. B. (1987). Petroleum engineering handbook. Society of Petroleum Engineers.

Buckley, S. E., & Leverett, M. C. (1942). Mechanism of fluid displacement in sands. Transactions of the Society of Petroleum Engineers of the American Institute of Mining, Metallurgical, and Petroleum Engineers, Inc, 146(01), 107–116. https://doi.org/10.2118/942107-g

Chen, Z., Huan, G., & Ma, Y. (2006). Computational methods for multiphase flows in porous media. Society for Industrial and Applied Mathematics, SIAM.

Cobb, W. M., & Marek, F. J. (1997). Determination of Volumetric Sweep Efficiency in Matura Waterfloods Using Production Data. SPE, 38902(2), 93–100.

Craig, F. F. (1971). The reservoir engineering aspects of waterflooding. Society of Petroleum Engineers.

Crawford, P. B. (1960). Factors affecting waterflood pattern performance and selection. Journal of Petroleum Technology, 12(12), 11–15. https://doi.org/10.2118/1503-g

Deppe, J. C. (1961). Injection Rates - The Effect of Mobility Ratio, Area Swept, and Pattern. SPE-1472-G. 1.

Dykstra, H., & Parsons, R. L. (1950). The prediction of oil recovery by waterflood. Secondary Recovery of Oil in the United States. 2, 160–174.

Farajzadeh, R., Zekri, A., & Skauge, A. (2022). Improved oil recovery techniques and their role in energy transition. Journal of Cleaner Production, 354.

Kimbler, O. K., & Caudle, B. H. (1964). Areal sweepout behavior in a nine-spot injection pattern. Journal of Petroleum Technology, 16(02), 199–202. https://doi.org/10.2118/784-pa

Liu, B., Chen, J., Zhang, N., Liu, J., Zhang, Y., Bao, H., Liu, L., & Chen, K. (2023). Optimized scheduling of an integrated energy system with an electric truck battery swapping station. Processes (Basel, Switzerland), 12(1), 84. https://doi.org/10.3390/pr12010084

Muggeridge, A., Cockin, A., Webb, K., Frampton, H., Collins, I., Moulds, T., & Salino, P. (2014). Recovery rates, enhanced oil recovery and technological limits. Philosophical Transactions. Series A, Mathematical, Physical, and Engineering Sciences, 372(2006), 20120320. https://doi.org/10.1098/rsta.2012.0320

Muskat, M. (1951). Physical principles of oil production: Reply to review. The Journal of Geology, 59(5), 513–515. https://doi.org/10.1086/625900

Nordbotten, J. M., Fernø, M. A., Flemisch, B., Kovscek, A. R., Lie, K.-A., Both, J. W., Møyner, O., Sandve, T. H., Ahusborde, E., Bauer, S., Chen, Z., Class, H., Di, C., Ding, D., Element, D., Firoozabadi, A., Flauraud, E., Franc, J., Gasanzade, F., ... Youssef, A. A. (2025). Benchmarking CO2 storage simulations: Results from the 11th Society of Petroleum Engineers Comparative Solution Project. In arXiv [physics.geo-ph]. http://arxiv.org/abs/2507.15861

Oliver, D. S., Reynolds, A. C., & Liu, N. (2008). Inverse theory for petroleum reservoir characterization. Cambridge University Press.

Petrov, S. M., Ibragimova, D. A., Safiulina, A. G., Tohidi Kalorazi, B., Vakhin, A. V., Okekwe, R. C., & Karalin, E. A. (2017). Conversion of organic matter in the carbonaceous medium in the supercritical water. Journal of Petroleum Science & Engineering, 159, 497–505. https://doi.org/10.1016/j.petrol.2017.09.060

Rawya, S., Alikhan, A. A., & Ali, F. (1989). Potential of Non-thermal Methods for Heavy Oil Recovery. J. Can. Petrol. Technol, 28, 45–59.

Raziperchikolaee, S., Cotter, Z., & Gupta, N. (2021). Assessing mechanical response of CO2 storage into a depleted carbonate reef using a site-scale geomechanical model calibrated with field tests and InSAR monitoring data. Journal of Natural Gas Science and Engineering, 86(103744), 103744. https://doi.org/10.1016/j.jngse.2020.103744

Rose, S. C., Buckwalter, J. F., & Woodhall, R. J. (1989). The Design Engineering Aspects of Waterflooding. Monograph Series.

Sheng, J. J. (2011). Modern chemical enhanced oil recovery: Theory and practice. Gulf Professional Publishing.

Thakur, G. C. (1998). The role of reservoir management in carbonate waterfloods. SPE India Oil and Gas Conference and Exhibition, 3.

Thomas, S. (2008). Enhanced oil recovery - an overview. Oil & Gas Science and Technology, 63(1), 9–19. https://doi.org/10.2516/ogst:2007060

Welge, H. J. (1952). A simplified method for computing oil recovery by gas or water drive. Journal of Petroleum Technology, 4(04), 91–98. https://doi.org/10.2118/124-g

 $(N.d.).\ Psu.edu.\ Retrieved\ October\ 31,\ 2025,\ from\ https://www.e-education.psu.edu/png301/node/642.$